

1
2
3
4
5
6
7
8
9
10
11
12
13
14
15
16
17
18
19
20
21
22
23
24
25
26
27
28
29
30
31
32
33
34
35
36
37
38
39
40
41
42
43
44
45

Temporal proteomic analysis of BK polyomavirus infection reveals virus-induced G2 arrest and highly effective evasion of innate immune sensing

Laura G. Caller^{†1}, Colin T.R. Davies^{†2}, Robin Antrobus², Paul J. Lehner², Michael P. Weekes^{*2},
Colin M. Crump^{*1}

¹ Division of Virology, Department of Pathology, University of Cambridge, Tennis Court Road, Cambridge, CB2 1QP, UK

² Cambridge Institute for Medical Research, Wellcome Trust MRC Building, Addenbrooke's Hospital, Hills Rd, Cambridge, CB2 0QQ, UK

[†] These authors contributed equally to this work

^{*} Corresponding authors: mpw1001@cam.ac.uk; cmc56@cam.ac.uk

46 **Abstract**

47 BK polyomavirus (BKPyV) is a small DNA virus that establishes a life-long persistent infection in
48 the urinary tract of most people. BKPyV is known to cause severe morbidity in renal transplant
49 recipients and can lead to graft rejection. The simple 5.2 kilobase pair dsDNA genome expresses
50 just seven known proteins, thus it relies heavily on host machinery to replicate. How the host
51 proteome changes over the course of infection is key to understanding this host:virus interplay.
52 Here for the first time quantitative temporal viromics has been used to quantify global changes in
53 >9,000 host proteins in two types of primary human epithelial cell throughout 72 hours of BKPyV
54 infection. These data demonstrate the importance of cell cycle progression and pseudo-G2 arrest in
55 effective BKPyV replication, along with a surprising lack of innate immune response throughout
56 the whole virus replication cycle. BKPyV thus evades pathogen recognition to prevent activation
57 of innate immune responses in a sophisticated manner.

58

59 **Importance**

60 BK polyomavirus can cause serious problems in immune-suppressed patients, in particular kidney
61 transplant recipients who can develop polyomavirus-associated kidney disease. In this work, we
62 have used advanced proteomics techniques to determine the changes to protein expression caused
63 by infection of two independent primary cell types of the human urinary tract (kidney and bladder)
64 throughout the replication cycle of this virus. Our findings have uncovered new details of a
65 specific form of cell cycle arrest caused by this virus and importantly we have identified that this
66 virus has a remarkable ability to evade detection by host cell defence systems. In addition, our data
67 provide an important resource for the future study of kidney epithelial cells and their infection by
68 urinary tract pathogens.

69 **Introduction**

70 BK Polyomavirus (BKPyV) is a small, non-enveloped, double stranded DNA virus that was first
71 identified in 1971 (1). As a ubiquitous pathogen, it establishes a life-long persistent infection in the
72 kidneys of most humans (2). While infection with BKPyV is subclinical in the vast majority of
73 individuals, it is a significant cause of morbidity in the immunosuppressed, in particular kidney
74 and haematopoietic stem cell transplants (HSCT) recipients. Polyomavirus associated nephropathy
75 (PVAN) affects ~8% of kidney transplant patients, however treatment is currently limited to a
76 reduction in immune suppression. Only a small number of anti-BKPyV drugs are available, all
77 exhibiting significant nephrotoxicity, leading to graft decline of function and loss in ~85% of
78 PVAN sufferers (3). In up to 15% of HSCT patients, BKPyV leads to haemorrhagic cystitis (HC)
79 and severely reduced rates of HSCT recovery (4).

80 As with all polyomaviruses, BKPyV is structurally simple. The dsDNA genome is ~5.2 kilobase
81 pairs long and encodes seven proteins, three of which form the virus capsid (VP1, VP2 and VP3).
82 The four non-structural proteins (large T antigen (LTA_g), small T antigen (stA_g), truncTAg and
83 agnoprotein) have numerous functions and interact with multiple host factors. For example, LTA_g
84 binds members of the Retinoblastoma protein family, inhibiting their regulation of the G1/S phase
85 checkpoint of the cell cycle. As a result, viral infection stimulates cell cycle progression into S
86 phase, facilitating viral DNA genome replication (5, 6). LTA_g also binds p53, altering the
87 regulation of both apoptosis and cell cycle progression (7). stA_g modulates the phosphorylation of
88 >300 cell cycle proteins and LTA_g, through interaction with protein phosphatase 2A (8, 9). The
89 role of agnoprotein is less well understood, although a wide range of activities have been proposed
90 including action as a viroporin, enhancing viral DNA replication through interaction with the
91 processivity factor proliferating cell nuclear antigen (PCNA), and enhancing egress of virions from
92 the nucleus (10, 11).

93 The limited coding capacity of BKPyV necessitates co-option of multiple host factors in order to
94 replicate and persist. Previous studies investigating how BKPyV infection modulates the host cell
95 environment have primarily been conducted at the level of the transcriptome, which may not be
96 reflected in the proteome. Infection in primary Renal Proximal Tubule Epithelial (RPTE) and
97 Human Umbilical Vein Endothelial (HUV-EC) cells has been studied, either using microarray (12,
98 13) or RNAseq (14, 15). Such analyses do not provide information about virus-induced changes to
99 cellular proteins. To date there has only been one limited analysis of changes to the host cell
100 proteome in BKPyV infection, where stable isotope labelling with amino acids in cell culture
101 (SILAC) was used to quantify protein changes in nuclei isolated from primary RPTE cells at 3

102 days post infection. In this study ~2000 proteins were quantified, and the effect of infection on
103 proteins outside the nucleus could not be assessed (16).

104 To gain a comprehensive global understanding of changes in host and viral proteins throughout the
105 whole course of BKPyV infection, we conducted a 10-plex quantitative temporal viromic analysis
106 (QTV) of two independent BKPyV-permissive primary human cell types, RPTE and human
107 urothelial (HU) cells. QTV uses tandem mass tags (TMT) and MS3 mass spectrometry to quantify
108 the relative abundance of proteins throughout the whole time course of infection (17). These data
109 have provide the broadest global analysis of proteome changes caused by BKPyV infection, which
110 has provided additional details of a specialised form of cell cycle arrest that is induced by this
111 virus in primary cells. In addition, we have uncovered a complete lack of induction of innate
112 immune responses at the protein level in BKPyV infected cells suggesting that this virus has
113 evolved a sophisticated mechanism for evading pathogen recognition.

114

115 **Results**

116 **Quantitative Temporal Viromic analysis of BKPyV infection**

117 To build a global picture of changes in host and viral proteins throughout the course of BKPyV
118 infection, we infected primary renal (RPTE) and bladder (HU) epithelial cells with BKPyV
119 Dunlop strain. We first used 10-plex TMT and MS3 mass spectrometry to quantify changes in
120 protein expression over three key time points of infection spanning the single-step replication
121 cycle of this virus (0-72 hours) (Experiment 1; Fig. 1A). Cells were infected at a multiplicity of
122 infection (MOI) of 5 infectious units per cell ensuring greater than 90% infection in both RPTE
123 and HU cells (data not shown). In this experiment a total of 8985 cellular and 5/7 viral proteins
124 were quantified in both cell types, providing a global view of changes in protein expression during
125 infection in primary human epithelial cells from the kidney and bladder. Data from all proteomic
126 experiments in this study are shown in Table S1. Here, the worksheet “Plots” is interactive,
127 enabling generation of graphs of protein expression of any of the human and viral proteins
128 quantified.

129 In uninfected cells, RPTE and HU cells exhibit differential expression of proteins, as expected
130 from two different cell types. In infected cells, few changes occurred by 24 h of infection, however
131 more substantial differences were seen by 48 and 72 h (Fig. 1B and C). In RPTE cells 191 cellular
132 proteins increased >2-fold, while 149 proteins decreased >2-fold at any time point during BKPyV
133 infection. In HU cells 130 proteins increased >2-fold and 55 decreased >2-fold. Many proteins

134 showed similar changes in both cell types, although cell type-specific effects were also seen (Fig.
135 1D; $R=0.61$). We reasoned that those protein changes which were important for viral replication
136 would be common to different cell types. By combining the two datasets, we found that just 86
137 cellular proteins, less than 1% of all proteins quantified, were upregulated >2-fold in both RPTE
138 and HU cells (Fig. 1D).

139 The lack of change in the host cell proteome at the earliest time point of 24 hpi suggested little or
140 no effect of virus binding and penetration. To investigate this further a second TMT-based whole
141 cell proteomics experiment (Experiment 2) was conducted repeating 24 and 48 hpi time points
142 with an additional earlier 12 hpi time point, where RPTE cells were infected with UV-inactivated
143 or unmodified BKPyV at MOI 5 (Fig. 2, Table S1). In Experiment 2 a total of 7698 cellular
144 proteins were quantified, some of which were not detected in Experiment 1, giving a combined
145 total of 9304 cellular proteins quantified across both experiments. Very few changes in protein
146 abundance were observed at 12 or 24 hpi during infection with unmodified BKPyV, while at 48
147 hpi cellular proteins upregulated were similar to those observed in the first experiment at the same
148 time point (Fig. 2B-D). UV-inactivated virus induced virtually no changes at any time point,
149 suggesting that virus replication is necessary to cause the observed changes in host protein
150 abundance (Fig. 2B).

151 **Temporal Analysis of BK Polyomavirus Protein Expression**

152 Expression of the early BKPyV proteins, LTA_g and stA_g, was observed from 24 hpi, closely
153 followed by late proteins, agnoprotein, VP1 and VP2. Profiles from HU and RPTE cells (both
154 experiments) corresponded well (Fig. 1E and 2E). We were unable to assign peptides to VP3 due
155 to its 100% sequence identity with the C terminus of VP2, and the single unique peptide
156 corresponding to the extreme N-terminus of VP3 was not quantified. Likewise, TruncTA_g was not
157 identified due to its similarity to full length LTA_g: the only difference in protein sequence are the
158 C-terminal 3 amino acids of TruncTA_g, which directly follow a cluster of lysine and arginine
159 residues and so would not be expected to be identified by our mass spectrometry analysis.

160 **BKPyV does not cause induction of innate immune responses in infected RPTE cells**

161 One surprising observation from our QTV analyses was an apparent lack of an innate immune
162 response to BKPyV infection. Of the 131 quantified proteins with annotated innate immune
163 functions or the 69 quantified proteins with annotated antiviral functions only five were up- or
164 downregulated >2-fold, and these changes were not consistent between the two independent cell
165 types or experiments (Fig. 3A and Table S2). Despite RPTE cells being capable of mounting a
166 response to type I interferon, the expression of interferon stimulated genes MX1, ISG15, IFIT1,

167 IFIT2, IFIT3, IRF3, IFI16, and BST2 remained unchanged upon BKPyV infection throughout the
168 time course, as assessed both by proteomics and Western blot (Fig. 3B and C). This was
169 unexpected given that by 72 hpi large amounts of viral DNA and proteins as well as progeny
170 virions were present within cells. This lack of response suggests BKPyV has evolved a highly
171 effective immune-evasion activity, which could be due to either viral DNA and proteins not being
172 recognised by host pathogen recognition receptors (PRRs) in these primary epithelial cells, or
173 suppression of PRR signalling pathways during BKPyV infection.

174 Activation of RNA and DNA sensors invariably leads to IRF3 phosphorylation and translocation
175 into the nucleus, leading to transcription of type I and III interferons. We analysed whether RPTE
176 cells have functional RNA and DNA sensing pathways, and whether these were activated in
177 response to BKPyV infection. The phosphorylation and localisation of IRF3 was investigated by
178 Western blot and immunofluorescence microscopy following BKPyV infection or treatment with
179 Poly I:C or stimulatory DNA. Poly I:C or stimulatory DNA caused clear nuclear translocation of
180 IRF3 in RPTE cells, with poly I:C having the greatest effect (Fig. 4A). However, BKPyV-infected
181 RPTE cells had no detectable change in IRF3 localisation and appeared no different to mock
182 infected cells apart from characteristic enlarged nuclei in virus infected cells (Fig. 4A).
183 Furthermore, Western blot analysis showed no stimulation of IRF3 phosphorylation in BKPyV-
184 infected RPTE cells, whereas both poly I:C and stimulatory DNA transfection caused robust IRF3
185 phosphorylation (Fig. 4B). These results suggest that signal transduction pathways that would
186 usually lead to activation of IRF3-specific kinases are not activated in infected cells either due to
187 an inability to sense BKPyV nucleic acids or due to active inhibition by BKPyV.

188 To investigate whether the lack of viral sensing is due to evasion of nucleic acid detection or active
189 suppression of IRF3 phosphorylation, RPTE cells were mock or BKPyV-infected and
190 subsequently stimulated with Poly I:C or stimulatory DNA at 42 hpi, prior to analysis at 48 hpi.
191 Nuclear translocation and robust phosphorylation of IRF3 was observed in response to both RNA
192 and DNA, irrespective of whether the cells were infected with BKPyV or mock-infected (Fig. 5A
193 and B). This suggests that BKPyV does not actively inhibit nucleic acid sensing pathways, IRF3
194 phosphorylation or IRF3 nuclear translocation. As BKPyV does not inhibit downstream activation
195 of RNA or DNA sensing pathways this suggests BKPyV evades nucleic acid and other pathogen
196 associated molecular pattern (PAMP) sensing pathways altogether, despite high concentrations of
197 viral DNA, RNA and protein within these primary renal epithelial cells.

198 **Cell cycle associated proteins are the primary target of BKPyV**

199 To investigate host cell functions that were modified by BKPyV, the Database for Annotation,
200 Visualisation and Integrate Discovery (DAVID) was used to identify pathways enriched among
201 proteins up- or downregulated during BKPyV infection (18). Amongst upregulated proteins,
202 similar terms were enriched between HU and RPTE cells (both from experiments 1 and 2). ‘Cell
203 cycle’ and terms related to the cell cycle dominated this analysis (Fig. 6A, Tables S3 and S4).
204 Terms associated with the G2/M phase of the cell cycle were particularly enriched, including:
205 chromosome, microtubule, spindle, sister chromatid cohesion and DNA damage. G2/M phase
206 arrest has previously been observed in a number of different polyomavirus infections (19-22).

207 Cellular proteins associated with G2/M phase of the cell cycle generally increased in abundance
208 throughout BKPyV infection including: M-phase (CDCA3), spindle formation (CDC20, CDCA2),
209 kinetochore assembly, sister chromatid segregation and cytokinesis (KIF11, CENPK, SKA1,
210 KIF22, ANLN), DNA repair and control of re-replication (HELLS, GMNN) and G2/M-associated
211 cyclins and cyclin-dependent kinases (CDK1, cyclin A2 and cyclin B1) (Fig. 6B). Proteins
212 associated with the G1 phase, such as cyclin D2, were observed to decrease in abundance. As
213 expected, levels of the tumour suppressor p53 were elevated during BKPyV infection;
214 polyomavirus LTA_g binds, stabilises and inactivates p53 (5, 23, 24). Interestingly, MDM2, the
215 ubiquitin ligase that normally mediates p53 degradation, was depleted during BKPyV infection
216 (Fig. 6B).

217 We confirmed these results for a number of cell cycle regulatory proteins by Western blot
218 throughout the time course of BKPyV infection in both RPTE and HU cells (Fig. 6C).
219 Immunofluorescence microscopy of BKPyV or mock-infected RPTE cells further confirmed the
220 increase in cyclin B1 and CDK1 during BKPyV infection, and furthermore that cyclin B1
221 remained cytoplasmic during BKPyV infection (data not shown). This suggests that infected cells
222 do not proceed into M phase, when cyclin B1 would normally localise to the nucleus (25).

223 **MDM2 and p53 levels are modulated by LTA_g and cell cycle arrest**

224 BKPyV-induced upregulation of p53 and downregulation of MDM2 was also confirmed by
225 immunofluorescence (Fig. 7). The E3 ubiquitin ligase MDM2 is a negative regulator of both p53
226 and itself, leading to ubiquitinylation and degradation of p53 and MDM2 (26). In addition, p53 is a
227 transcription factor for both itself and MDM2 (27), whose transcriptional activity is governed by
228 the strength of extracellular and intracellular signals, such as cell cycle checkpoints, leading to the
229 establishment of both positive and negative feedback loops (28).

230 Polyomavirus LTA_gs are well established to efficiently bind, stabilise and inhibit p53 (5, 23, 24),
231 leading to increased p53 levels in BKPyV infected cells. Our data now demonstrates that this is

232 accompanied by a decrease in MDM2 levels. Interplay between BKPyV infection, MDM2 and p53
233 was investigated using the MDM2 inhibitor Nutlin-3. Nutlin-3 occupies the p53 binding pocket on
234 MDM2 obstructing their interaction and leading to reduced p53 ubiquitinylation. In addition,
235 Nutlin-3 leads to increased transcription of MDM2 due to the release of active p53 (29). Mock or
236 BKPyV infected RPTE cells were treated with Nutlin-3 at 2 hpi, or DMSO as a control, and fixed
237 at 48 hpi. Cells were immunostained for expression of MDM2, p53, and LTA_g (infection marker)
238 (Fig. 7A). Low endogenous levels of both MDM2 and p53 were observed in the nuclei of
239 untreated mock infected cells. BKPyV infection lead to a reduction in MDM2, while p53
240 increased, correlating with the changes observed in the proteomics data. Mock infected cells
241 treated with Nutin-3 showed increased levels of MDM2, accompanied by a slight increase in p53
242 levels, in accordance with published effects of Nutlin-3 (29). Interestingly, MDM2 levels did not
243 increase in BKPyV infected cells treated with Nutlin-3 and in fact MDM2 levels were observed to
244 reduce, whilst p53 levels were once again increased. This suggests that during infection MDM2
245 remains able to self-ubiquitinylate, leading to its degradation in the presence of Nutlin-3, however
246 transcription of MDM2 by p53 is apparently inhibited, likely due to p53 sequestration by LTA_g.

247 To investigate whether LTA_g expression alone was sufficient to cause the observed MDM2
248 decrease and p53 increase RPTE cells were transfected with a LTA_g expression plasmid. At 2 h
249 cells were treated with Nutlin-3 or DMSO and then in addition some samples were treated at 24 h
250 with a CDK1-specific inhibitor, RO-3306, to simulate BKPyV induced cell cycle arrest. Cells
251 were fixed at 48 h and immunostained for MDM2, p53, and LTA_g (Fig. 7B). Expression of LTA_g
252 alone was sufficient to reduce MDM2 levels, however p53 levels were increased only slightly
253 suggesting other effects of BKPyV infection in addition to LTA_g expression modulate p53 and
254 MDM2 levels. Nutlin-3 treatment did not alter the effects of LTA_g on MDM2 or p53 levels.
255 Treatment of LTA_g expressing cells with the CDK1 inhibitor RO-3306 lead to a marked increase
256 in p53 expression, while MDM2 levels were once again decreased. Combined Nutlin-3 and RO-
257 3306 treatment further enhanced the increase of p53 in LTA_g expressing cells. Taken together,
258 these data suggest LTA_g binding to p53 displaces MDM2 leading to p53 stabilisation and MDM2
259 degradation, but LTA_g binding also prevents p53-dependent expression of MDM2 and p53.
260 Furthermore, virus infection or G2/M arrest stimulates p53 expression, possibly via a DNA
261 damage-type response.

262 **BKPyV induced G2/M phase arrest is prevented by inhibition of CDK1 & CDK2, but not by**
263 **inhibition of CDK1 alone or CDK4 & CDK6**

264 Given the dysregulation of cell cycle-related proteins during BKPyV replication, we postulated
265 that a virus-induced pseudo-G2 phase may serve a number of roles in BKPyV replication. We

266 therefore investigated the effect of BKPyV infection on the host cell cycle status in the presence or
267 absence of various CDK inhibitors. Polyomavirus replication is heavily reliant on the host DNA
268 synthesis machinery and it has previously been shown that either BKPyV infection or JCPyV
269 LTA_g expression alone can cause cells to arrest in the G2/M phase of the cell cycle (22, 30, 31).
270 However, the impact of CDK inhibitors on BKPyV-induced arrest has not been fully investigated.
271 RPTE cells were infected with BKPyV, treated with CDK inhibitors after 24 hpi to allow
272 sufficient time for virus entry and initiation of early gene expression, then subsequently harvested
273 at 48 hpi and analysed by flow cytometry to compare cell cycle profiles. PD0332991 was used to
274 inhibit CDK4 and 6, which are active in G1 phase, Roscovitine was used to inhibit CDK1 and 2,
275 which are active throughout S, G2, and M phase, and RO-3306 was used to inhibit CDK1, which
276 is active in G2 and M phase. In mock-infected RPTE cells, all three inhibitors produced the
277 expected effects: PD0332991 increased the proportion of cells in G1 from 72% to 84% ($p < 0.05$),
278 Roscovitine showed little change in proportion of cells in any cell cycle phase because of its broad
279 effect on S, G2 and M phases, and RO-3306 showed an increased proportion of cells in G2/M
280 (18% to 23%) and reduced proportion in G1 (72% to 65%), although this did not reach statistical
281 significance (Fig. 8A and B). Cell viability remained above 90% for all inhibitor conditions used
282 (Fig. 8C). Infection of RPTE cells with BKPyV in the absence of any inhibitor significantly
283 increased the proportion of cells in G2/M from 18% to 31% and decreased the proportion of cells
284 in G1 (72 % to 56%; $p < 0.01$), consistent with BKPyV-induced G2 arrest observed in previous
285 published data (30). BKPyV-infected cells that were treated with PD0332991 showed a significant
286 decrease in the proportion of cells in G1 compared to uninfected cells treated with PD0332991
287 (84% to 58%; $p < 0.001$). While a slight increase was observed in the proportion of cells in G1 for
288 BKPyV infected and PD0332991 treated cells compared to control BKPyV infected cells (56% to
289 58%) this did not reach statistical significance. This suggests that inhibition of CDK4 and 6 does
290 not prevent BKPyV driving infected cells through the G1/S checkpoint (due to Rb inactivation by
291 LTA_g) or arresting cells in G2/M. In contrast, treatment of infected cells with Roscovitine, which
292 inhibits both CDK1 and 2, appears to severely restrict BKPyV-stimulated S phase entry and G2/M
293 arrest, as the cell cycle status was similar to that of mock-infected cells with no significant change
294 in the proportion of cells in any cell cycle phase. BKPyV infected cells treated with RO-3306
295 (CDK1 inhibitor) showed a similar cell cycle profile to that of control BKPyV infected cells, with
296 no significant difference in the proportion of cells in any cell cycle phase (Fig. 8A). Comparison of
297 mock infected RO-3306 treated cells with BKPyV infected RO-3306 treated cells showed
298 increased proportion of cells in G2/M and S with a corresponding decrease in G1 (65% to 49%;
299 $p < 0.05$). This suggests that BKPyV infection and CDK1 inhibition have a similar and additive
300 effect on the cell cycle, namely induction of G2/M arrest.

301 **Inhibition of CDK1 and CDK2 or CDK1 alone reduces BKPyV replication**

302 The ability of BKPyV to induce a pseudo-G2 arrest in the presence of CDK1 or CDK4/6 inhibition
303 suggested that virus replication should be unaffected in such conditions, while inhibition of
304 CDK1/2 should perturb viral replication due to inhibition of S phase progression. To investigate if
305 this was the case we next analysed the effect of CDK inhibitors on viral genome synthesis in
306 BKPyV infected RPTE cells. Infected cells were treated with each inhibitor at 24 hpi and
307 harvested at 48 hpi. Viral and host cell DNA was quantified using qPCR to determine viral DNA
308 copy numbers per cell and were normalised to uninhibited controls (arbitrarily set to 1). Inhibition
309 of CDK4/6 had no significant effect on viral genome synthesis, while inhibition of CDK1 and 2 by
310 Roscovitine showed a 7.4-fold reduction in the synthesis of BKPyV genome, likely due to the
311 restriction of cells from entering and progressing through S phase (Fig. 9A). Surprisingly,
312 inhibition of CDK1 alone by RO-3306 also caused a significant, although more modest, 2.3-fold
313 reduction in BKPyV genome synthesis. This suggests that, despite this inhibitor having little effect
314 on BKPyV-driven cell cycle progression, CDK1 activity is important for efficient viral genome
315 synthesis.

316 The effects of these CDK inhibitors on viral protein synthesis was similarly investigated (Fig. 9B).
317 Inhibition of CDK4 and 6 had no observable effect on viral protein synthesis, while inhibition of
318 CDK1 and 2 by Roscovitine substantially reduced viral protein expression levels. Inhibition of
319 CDK1 alone by RO-3306 showed only small reductions in viral protein levels.

320 Analysis of infectious virus production in the presence or absence of these CDK inhibitors also
321 demonstrated a similar trend. Inhibition of CDK4 and 6 caused only a slight reduction of
322 infectious titres, whereas inhibition of CDK1 and 2 by Roscovitine resulted in a significant 80-fold
323 reduction of virus production, unsurprisingly given the inhibition of viral DNA and protein
324 synthesis (Fig. 9C). Inhibition of CDK1 alone by RO-3306 caused a significant reduction of
325 infectious virus titre by >3-fold. These data further suggest that CDK1 activity is important for the
326 efficient production of infectious viruses.

327

328 **Discussion**

329 By employing the power and sensitivity of TMT-based MS3 mass spectrometry technology, we
330 have been able to uncover BKPyV-induced changes to protein abundance and a global view of
331 protein expression within these human cell types. Importantly, these studies were conducted in
332 primary human cells from epithelial tissue representing the natural sites of replication *in vivo*.

333 Therefore, this work also provides a comprehensive proteomic resource for future studies on
334 human renourinary epithelial biology.

335 One of the most surprising findings of this study was just how few of the ~9000 cellular proteins
336 that were quantified changed in abundance in response to BKPyV infection. In fact, just 235 were
337 found to be upregulated and 196 downregulated >2-fold or more across either cell type at any time
338 point, which corresponds to <5% of the total proteome. Previous studies that applied a similar
339 TMT-based approach to infection with human cytomegalovirus (HCMV), another dsDNA virus,
340 revealed that 56% of cellular proteins changed in abundance more than 2-fold during the course of
341 infection (17). This suggests that BKPyV, and presumably other polyomaviruses, are so highly
342 adapted to their host that they only need to induce subtle changes to host gene expression to
343 reprogram cells into virus-producing factories. This also suggests polyomaviruses can very
344 effectively evade detection by host pathogen recognition receptors despite producing high
345 concentrations of foreign (viral) nucleic acid and proteins during productive infection.

346 For host proteins induced by BKPyV infection, we identified substantial overlap between the two
347 primary cell types, with many of the same or highly related functional clusters identified by
348 DAVID analysis. This includes clusters such as ‘DNA damage’ and the ‘Fanconi Anaemia’
349 pathway, which have been previously described as important during polyomavirus replication to
350 ensure viral genome replication maintains high fidelity (30). Interestingly, the majority of the
351 functional clusters identified as upregulated in BKPyV infection are related to cell cycle activity
352 and regulation, in particular activities associated with G2 and M phases. In fact, BKPyV infection
353 appears to have a similar ‘G2/M arrest’ effect on cell cycle status as the CDK1-specific inhibitor
354 RO-3306, a drug commonly used to arrest cells in G2. The fact that infected cells do not progress
355 into authentic mitosis is supported by the observation that cyclin B1 remains predominantly
356 cytoplasmic despite higher protein levels in infected cells, and supports previously published data
357 indicating G2/M phase arrest is driven by polyomavirus infection (5-7, 22, 32). Our data now
358 provides a greater understanding of host protein profiles that are associated with polyomavirus-
359 induced G2 arrest, and it would be interesting to compare these observations to the effects of RO-
360 3306 or other specific CDK1 inhibitors on cellular protein expression profiles.

361 Our data also indicate a specific perturbation of the p53-MDM2 axis by BKPyV infection, where
362 MDM2 is reduced and p53 is increased but kept inactive by LTA_g binding. However, these
363 changes require more than just LTA_g expression, and are also driven by additional effects of
364 BKPyV infection related to G2/M arrest and potentially DNA damage responses. Our findings
365 suggest the following model: low MDM2 and p53 levels are maintained in uninfected cells due to
366 their poly-ubiquitinylation by MDM2 and subsequent proteosomal degradation (Fig. 10A).

367 Inhibition of MDM2-p53 interaction by Nutlin-3 releases p53 which then stimulates MDM2
368 expression (Fig. 10B). Interaction of LTA_g with p53 displaces MDM2, thereby causing MDM2 to
369 be destroyed by the proteasome, and so protects p53 from degradation but inhibits p53
370 transcriptional activity prevent induction of de novo MDM2 expression (Fig. 10C). Therefore, the
371 expression of just LTA_g results in decreased MDM2 levels but only a modest increase in p53.
372 During active BKPyV infection, p53 expression is induced by some other effect(s) of virus
373 replication, and these additional copies of p53 are also bound and inactivated by LTA_g (Fig. 10D).
374 We predict that stimulation of p53 expression during BKPyV infection is via a DNA damage
375 response pathway, which can be mimicked by inducing a G2 arrest through inhibition of CDK1.

376 Polyomaviruses have a well-established capacity to drive cells into S-phase by overriding the G1/S
377 checkpoint via the activity of LTA_g. It is therefore unsurprising that inhibition of CDK4 and 6 has
378 little-to-no effect on the ability of BKPyV to drive cell cycle progression or to replicate. CDK4
379 and 6, in complex with cyclin D, are normally responsible for phosphorylation of Rb and release
380 of E2F proteins allowing passage through the G1/S checkpoint (33). This is bypassed through the
381 binding of LTA_g to Rb family proteins, releasing E2F proteins enabling S-phase entry that is
382 unconstrained by upstream factors (5, 6).

383 In contrast Roscovitine, a potent inhibitor of CDK1 and 2, caused a global cell cycle arrest,
384 irrespective of BKPyV infection, and reduced BKPyV replication. Similar effects of Roscovitine
385 on polyomavirus replication have been previously been attributed to inhibition of CDK1 activity
386 alone (34). However, our data suggests the effect of Roscovitine are more likely due to inhibition
387 of CDK2 activity, or the combination of inhibiting both CDK1 and 2. Inhibition of both these
388 cyclin dependent kinases causes a rather global block to cell cycle progression; CDK2 is active in
389 both late G1 and S phase, while CDK1 is active in G2 and M phase (35). CDK2 activity is
390 required immediately after G1 checkpoint clearance and beyond, and so the primary cause of
391 BKPyV inhibition by Roscovitine could be due to a failure to activate S-phase proteins required
392 for viral genome synthesis and consequent protein expression. Interestingly, we also observed
393 reduced expression of LTA_g in Roscovitine treated cells. This might be attributed to inhibited
394 progression through S phase, thus leading to reduced viral genome copy numbers from which
395 LTA_g is transcribed, although other effects of Roscovitine that inhibit transcription, such as
396 inhibition of CDK7 and 9, may also contribute to this effect (36)

397 Somewhat more intriguing is the effect of CDK1-specific inhibition on BKPyV infection; RO-
398 3306 caused significant reductions in viral DNA synthesis and infectious virus assembly. This was
399 surprising because CDK1 activity is normally important for the transition through G2 and into M-
400 phase, and so inhibition of CDK1 would not be expected to inhibit progression through S-phase

401 and thus viral DNA replication. Whether CDK1 activity is required directly or indirectly to
402 enhance DNA synthesis or other S-phase activities required for BKPyV genome replication, or the
403 process of virion assembly, remains to be determined.

404 Moreover, our data have demonstrated that BKPyV infection of renourinary epithelial cells does
405 not appear to cause the induction of antiviral responses in agreement with published data of RPTE
406 cells (12, 14, 15). Both RPTE and HU cells express the appropriate receptors, signalling pathways
407 and transcription factors associated with sensing and responding to DNA viruses, such as cGAS
408 (MB21D1), IFI16, STING (TMEM173), NF κ B, and IRF3, which were readily detected in our
409 mass spectrometry analysis (Table S1). RPTE cells are quite capable of responding to foreign
410 intracellular DNA or RNA, leading to phosphorylation and nuclear translocation of IRF3, and
411 RPTE cells also robustly express antiviral genes in response to type-1 interferon. However, we
412 could not detect activation of these pathways even by three days after BKPyV infection: IRF3
413 remains unphosphorylated and cytoplasmic and no ISGs were induced. Furthermore, we have also
414 shown that active BKPyV infection within the same cell does not prevent the phosphorylation and
415 nuclear translocation of IRF3 in response to either cytoplasmic RNA or DNA. This suggests that
416 BKPyV is not actively suppressing such antiviral responses, but rather prevents its own detection
417 by pathogen recognition receptors. This evasion of detection may be due to a combination of
418 having a small circular double stranded DNA genome that is associated with histones, thus
419 appearing similar to open chromatin, and tightly regulated entry and egress mechanisms to prevent
420 exposure of viral DNA in the cytoplasm. Whether an inability to sense and respond to BKPyV
421 infection is partly due to the nature of epithelial cells in the renourinary systems and whether this
422 contributes to the natural tropism of BKPyV for these tissue types will be interesting questions for
423 future study.

424 In summary, we have generated extensive data sets on the protein expression profiles of primary
425 epithelial cells of the kidney and bladder using advanced multiplexed proteomics and provided a
426 detailed understanding of how infection by BKPyV modifies the protein expression profiles in
427 these cells. This research has provided additional details of the specific cell cycle arrest induced by
428 virus infection and revealed the importance of this arrest for BKPyV replication. Furthermore, our
429 findings suggest a surprising ability of BKPyV to evade detection and activation of innate immune
430 responses in cells that are natural sites of lytic virus infection *in vivo*.

431

432 **Materials and Methods**

433 **Cell types, virus and primary antibodies.**

434 HU cells were grown in Urothelial Cell Medium enriched with Urothelial Cell Growth
435 Supplement and penicillin/streptomycin solution (Caltag Medsystems). HU cells were used at
436 passage 4-6 for all experiments. RPTE cells were grown in renal epithelial basal media enriched
437 with REGM bullet kit (Lonza). RPTE cells were used at passage 6-7 for all experiments.

438 BKPyV (Dunlop strain) inserted into pGEM7Zf(+) vector (kindly provided by M. Imperiale,
439 University of Michigan) was digested with BamHI, purified and re-ligated. Resultant BKPyV-
440 Dunlop genome was transfected into a T150 flask of RPTE cells, one week later the flask was split
441 into three T150 flasks of RPTE cells. After a period of up to four weeks virus was harvested by
442 freeze thawing cells three times. Virus purification by sucrose cushion, followed by caesium
443 chloride gradient and dialysis provided purified BKPyV stocks as described previously (37).
444 Concentration and purity was assessed by FFU assay and coomassie gel stain respectively.

445 The primary antibodies used in this study were PAb597 against SV40 VP1 (kindly provided by W.
446 Atwood, Brown University), P5G6 against BKPyV VP1 (kindly provided by D. Galloway, Fred
447 Hutchinson Cancer Research Center), ab6160 against Tubulin (Abcam), ab32386 against Cyclin
448 A2 (Abcam), ab32053 against Cyclin B1 (Abcam), MA5-11472 against CDK1 (Thermo
449 Scientific), ab207604 against Cyclin D2, ab1101 against p53 (Abcam), GTX116125 against
450 Geminin (GeneTex), ab16895 against MDM2 (Abcam), 37849 against MX1 (Cell Signalling
451 Technologies), 2758 against ISG15 (Cell Signalling Technologies), PA3-848 against IFIT1
452 (ThermoFisher), 12604-1-AP against IFIT2 (ProteinTech), SAB1410691 against IFIT3 (Sigma
453 Aldrich), 11904 against IRF3 (Cell Signalling Technologies), ab76493 against IRF3 (phospho
454 S386) (Abcam), ac-8023 against IFI16 (Santa Cruz), 11721 against BST2 (NIH AIDS Reagent
455 Programme), ab53983 against SV40 VP2 + VP3 (Abcam), ab16879 against SV40 LTag (Abcam),
456 and against BKPyV agnoprotein (rabbit polyclonal antibody generated against agnoprotein
457 specific peptide).

458 **Cell infections and harvesting virus**

459 For viral infections RPTE or HU cells were infected with BKPyV at either MOI=5 for TMT and
460 validation experiments, or MOI=3 or 0.5 for all other experiments, diluted in appropriate medium.
461 At 1 hpi media was removed, cells washed twice with PBS and fresh medium was added. For
462 TMT analysis, cells were harvested in TMT lysis buffer (6M Guanidine HCl, 50mM HEPES pH
463 8.5), vortexed extensively and incubated at room temperature for 10 min. Lysates were then
464 sonicated at 25 W for 30 s, followed by centrifugation at 21,000 g for 10 min, after which
465 supernatant was transferred to a fresh tube. Centrifugation was repeated and supernatants snap-

466 frozen in liquid nitrogen for further processing. For Western blot, cells were harvested by
467 centrifugation at 6,000 g after two PBS washes.

468 **Transfection**

469 RPTE cells were transfected with pcDNA3-LTAg plasmid using TransIT-LT1 Transfection
470 Reagent (Mirus) in Opti-MEM media according to the manufacturers protocol.

471 **Inhibitors**

472 For p53:MDM2 interaction inhibition experiments cells were treated at 2 hpi with Nutlin-3.
473 Nutlin-3 (Sigma) was made up to 20mM in DMSO and used at 5 μ M. For cell cycle inhibition
474 experiments cells were treated with inhibitors at 24 hpi. PD0332991 (Sigma) was made up to 5mM
475 in dH₂O and used at 1 μ M, Roscovitine (Sigma) was made up to 20mM in DMSO and used at
476 20 μ M and RO-3306 (Sigma) was made up to 20mM in DMSO and used at 5 μ M. Controls were
477 subjected to treatment with an equivalent amount of DMSO at the greatest volume of any inhibitor
478 used. Cells were harvested in 1mL media at 48 hpi and either pelleted by centrifugation at 6,000 g
479 for use in Western blot or qPCR, or frozen for assay by FFU. For analysis by flow cytometry cells
480 were detached from wells by trypsin/EDTA treatment, centrifuged at 6,000 g, washed in PBS and
481 fixed in 70% ice-cold ethanol.

482 **FFU and immunofluorescence microscopy**

483 Fluorescent focus unit (FFU) assays were used to determine the concentration of infectious virus
484 in purified BKPyV stocks or experimental samples. RPTE cells were infected with sample
485 dilutions, fixed at 48 hpi and immunostained for VP1 expression as described in (38). For
486 comparison of inhibitor effects infectious BKPyV levels of uninhibited conditions were arbitrarily
487 set to 1 and inhibited conditions corrected to this control for 7 independent experiments. A one
488 sample t-test was conducted to give *p* values, standard deviation shown with error bars.

489 For immunofluorescence analysis, RPTE cells were fixed in 3% formaldehyde. Fixed cells were
490 then permeabilised and quenched (50mM NH₄Cl and 0.1% Triton X-100 in PBS), blocked in
491 PGAT (0.2% gelatin, 0.01% Triton X-100, 0.02% NaN₃ in PBS) and stained with primary
492 antibodies. Secondary antibodies used for immunofluorescence were Alexa Fluor 568 donkey anti-
493 mouse or goat anti-IgG1 mouse and Alexa Fluor 488 donkey anti-rabbit or goat anti-IgG2a mouse.
494 Coverslips were mounted using SlowFade Gold with DAPI (Invitrogen). Samples were imaged
495 using a 63x oil immersion lens on an Olympus IX81 wide-field fluorescent microscope.

496 **Western blot**

497 RPTE cells were lysed by suspending in mRIPA (50mM Tris pH 7.5, 150mM NaCl, 1% Sodium
498 Deoxycholate and 1% Triton X-100) supplemented with Complete Protease Inhibitors without
499 EDTA (Roche). Cellular debris were removed by centrifugation at 17,000g. HU cells were lysed
500 by suspending in HU cell Lysis Buffer (20mM HEPES pH 7.6, 250mM Sucrose, 2mM DTT, 2mM
501 EDTA Na₂ and 2mM EGTA) supplemented with Complete Protease Inhibitors without EDTA,
502 followed by sonication at 25W for 30 sec. Proteins were separated by SDS-PAGE electrophoresis
503 and transferred to nitrocellulose membranes before blocking in 5% skimmed milk powder in PBS.
504 Following primary antibody binding, LI-COR IRDye680- (anti-mouse, anti-rabbit or anti-rat) or
505 IRDye800-conjugated (anti-mouse or anti-rabbit) secondary antibodies were used. Membranes
506 were then imaged on a LI-COR Odyssey Infrared Imaging system.

507 **Real-time PCR (qPCR)**

508 RPTE cell pellets were lysed in 200 μ L NDA Lysis Buffer (4M Guanidine Thiocyanate, 25mM
509 Tris and 134mM β -mercaptoethanol) and incubated at 56°C for 10 min, after which an equal
510 volume of 100% ethanol was added. DNA was then bound to silica columns by centrifuging at
511 16,000 \times g for one min. Columns were washed with Buffer 1 (1M Guanidine Thiocyanate, 25mM
512 Tris pH7 in 10% ethanol), and centrifuged, followed by a final wash in Buffer 2 (25mM Tris pH7
513 in 70% ethanol). DNA was eluted with nuclease free water by centrifugation at 16,000 \times g. Primers
514 and probe for BKPyV genome were designed as described in (38). Human TNF α primers and
515 probe were designed and obtained through TIB MOLBIOL (forward primer:
516 AGGAACAGCACAGGCCTTAGTG; reverse primer: AAGACCCCTCCCAGATAGATGG;
517 Taqman probe: CCAGGATGTGGAGAGTGAACCGACATG). 300nM of each primer and 50nM
518 of Taqman probe were used in each qPCR reaction, run on a Rotor-Gene (RG-3000, Corbett
519 Research) and subsequently analysed on Rotor-Gene software. BKPyV genome levels were
520 corrected to the TNF α control for each sample, and uninhibited samples arbitrarily set to 1, 6
521 independent experiments. A one sample t-test was conducted to give *p* values, standard deviation
522 shown with error bars.

523 **Flow cytometry**

524 Cellular DNA content was used as an indicator of cell cycle status. Cells were fixed in 70%
525 ethanol for 30 mins, DNA was stained by resuspending each PBS washed cell pellet in 0.2mg
526 RNase A and 50 μ g propidium iodide in 1mL PBS and incubated at 37°C for 1 hr. Cells were then
527 centrifuged at 6,000 g, supernatant removed and resuspended in 500 μ L PBS. Cells were analysed
528 by flow cytometry using BD FACSCantoII with BD FACSDiva Software (BD Biosciences) and
529 further analysed using FlowJo v10.4.2 cell cycle analysis function. A minimum of 10,000 cells

530 were collected for each sample, 3 independent experiments. Two-tailed students t-tests were
531 conducted to assess significance of changes in cell cycle status between samples. Standard
532 deviation error was calculated for each cell cycle status sample.

533 **Whole cell lysate protein digestion**

534 Cells were washed twice with PBS, and 250 μl lysis buffer added (6M Guanidine/50 mM HEPES
535 pH 8.5). Cell lifters (Corning) were used to scrape cells in lysis buffer, which was removed to an
536 eppendorf tube, vortexed extensively then sonicated. Cell debris was removed by centrifuging at
537 21,000 g for 10 min twice. Dithiothreitol (DTT) was added to a final concentration of 5 mM and
538 samples were incubated for 20 mins. Cysteines were alkylated with 14 mM iodoacetamide and
539 incubated 20 min at room temperature in the dark. Excess iodoacetamide was quenched with DTT
540 for 15 mins. Samples were diluted with 200 mM HEPES pH 8.5 to 1.5 M Guanidine followed by
541 digestion at room temperature for 3 h with LysC protease at a 1:100 protease-to-protein ratio.
542 Samples were further diluted with 200 mM HEPES pH 8.5 to 0.5 M Guanidine. Trypsin was then
543 added at a 1:100 protease-to-protein ratio followed by overnight incubation at 37°C. The reaction
544 was quenched with 5% formic acid, then centrifuged at 21,000 g for 10 min to remove undigested
545 protein. Peptides were subjected to C18 solid-phase extraction (SPE, Sep-Pak, Waters) and
546 vacuum-centrifuged to near-dryness.

547 **Peptide labelling with tandem mass tags**

548 In preparation for TMT labelling, desalted peptides were dissolved in 200 mM HEPES pH 8.5.
549 Peptide concentration was measured by microBCA (Pierce), and 25 μg labelled with TMT reagent.
550 TMT reagents (0.8 mg) were dissolved in 43 μl anhydrous acetonitrile and 3 μl added to peptide at
551 a final acetonitrile concentration of 30% (v/v). Samples were labelled as follows. Experiment 1 (9-
552 plex); 126 – mock infection 12 hpi, 127N – mock infection 24 hpi, 127C – mock infection 48 hpi,
553 128N – BKPyV infection 12 hpi, 128C – BKPyV infection 24 hpi, 129N – BKPyV irradiated – 48
554 hpi, 129C – BKPyV irradiated 24 hpi, 130N BKPyV infection 48 hpi. Experiment 2 (10-plex); 126
555 – HU cells mock infection 24 hpi, 127N – HU cells mock infection 72 hpi, 127C – HU cells
556 BKPyV infection 24 hpi, 128N – HU cells BKPyV infection 48 hpi, 128C – HU cells BKPyV
557 infection 72 hpi, 129N – RPTE cells mock infection 24 hpi, 129C – RPTE cells mock infection 72
558 hpi, 130N – RPTE cells BKPyV infection 24 hpi, 130C – RPTE cells BKPyV infection 48 hpi,
559 131N – RPTE cells BKPyV infection 72 hpi. Following incubation at room temperature for 1 h,
560 the reaction was quenched with hydroxylamine to a final concentration of 0.3% (v/v). TMT-
561 labelled samples were combined at a 1:1:1:1:1:1:1:1:1 ratio (experiment 1) and 1:1:1:1:1:1:1:1:1
562 ratio (experiment 2). The sample was vacuum-centrifuged to near dryness and subjected to C18

563 SPE (Sep-Pak, Waters). An unfractionated singleshot was initially analysed to ensure similar
564 peptide loading across each TMT channel, to avoid the need for excessive electronic
565 normalization. Quantities of each TMT labelled sample were adjusted prior to high pH reversed-
566 phase (HpRP) so that normalisation factors were >0.67 and <1.5 . Normalisation is discussed in
567 'Data Analysis', and fractionation is discussed below.

568 **Offline HpRP fractionation**

569 TMT-labelled tryptic peptides were subjected to HpRP fractionation using an Ultimate 3000
570 RSLC UHPLC system (Thermo Fisher Scientific) equipped with a 2.1 mm internal diameter (ID)
571 x 25 cm long, 1.7 μm particle Kinetix Evo C18 column (Phenomenex). Mobile phase consisted of
572 A: 3% acetonitrile (MeCN), B: MeCN and C: 200 mM ammonium formate pH 10. Isocratic
573 conditions were 90% A / 10% C, and C was maintained at 10% throughout the gradient elution.
574 Separations were conducted at 45°C. Samples were loaded at 200 $\mu\text{l}/\text{minute}$ for 5 minutes. The
575 flow rate was then increased to 400 $\mu\text{l}/\text{minute}$ over 5 minutes, after which the gradient elution
576 proceed as follows: 0-19% B over 10 minutes, 19-34% B over 14.25 minutes, 34-50% B over 8.75
577 minutes, followed by a 10 minutes wash at 90% B. UV absorbance was monitored at 280 nm and
578 15 s fractions were collected into 96 well microplates using the integrated fraction collector.
579 Fractions were recombined orthogonally in a checkerboard fashion, combining alternate wells
580 from each column of the plate into a single fraction, and commencing combination of adjacent
581 fractions in alternating rows. Wells prior to the start or after the stop of elution of peptide-rich
582 fractions, as identified from the UV trace, were excluded. This yielded two sets of 12 combined
583 fractions, A and B, which were dried in a vacuum centrifuge and resuspended in 10 μl MS solvent
584 (4% MeCN / 5% formic acid) prior to LC-MS3. 11 set 'A' fractions were used for experiment 1
585 and 10 set 'A' fractions were used for experiment 2.

586 **LC-MS3**

587 Mass spectrometry data was acquired using an Orbitrap Lumos (Thermo Fisher Scientific, San
588 Jose, CA). An Ultimate 3000 RSLC nano UHPLC equipped with a 300 μm ID x 5 mm Acclaim
589 PepMap μ -Precolumn (Thermo Fisher Scientific) and a 75 μm ID x 50 cm 2.1 μm particle
590 Acclaim PepMap RSLC analytical column was used.

591 Loading solvent was 0.1% formic acid (FA), analytical solvent A: 0.1% FA and B: 80% MeCN +
592 0.1% FA. All separations were carried out at 55°C. Samples were loaded at 5 $\mu\text{L}/\text{minute}$ for 5
593 minutes in loading solvent before beginning the analytical gradient. The following gradient was
594 used: 3-7% B over 3 minutes, 7-37% B over 173 minutes, followed by a 4 minute wash at 95% B
595 and equilibration at 3% B for 15 minutes. Each analysis used a MultiNotch MS3-based TMT

596 method (39, 40). The following settings were used Th, 120,000 Resolution, 2×10^5 automatic gain
597 control (AGC) target, 50 ms maximum injection time. MS2: Quadrupole isolation at an isolation
598 width of m/z 0.7, CID fragmentation (normalised collision energy (NCE) 35) with ion trap
599 scanning in turbo mode from m/z 120, 1.5×10^4 AGC target, 120 ms maximum injection time.
600 MS3: In Synchronous Precursor Selection mode the top 6 MS2 ions were selected for HCD
601 fragmentation (NCE 65) and scanned in the Orbitrap at 60,000 resolution with an AGC target of
602 1×10^5 and a maximum accumulation time of 150 ms. Ions were not accumulated for all
603 parallelisable time. The entire MS/MS/MS cycle had a target time of 3 s. Dynamic exclusion was
604 set to ± 10 ppm for 70 s. MS2 fragmentation was triggered on precursors 5×10^3 counts and above.

605 **Data analysis**

606 In the following description, we list the first report in the literature for each relevant algorithm.
607 Mass spectra were processed using a Sequest-based software pipeline for quantitative proteomics,
608 “MassPike”, through a collaborative arrangement with Professor Steve Gygi’s laboratory at
609 Harvard Medical School. MS spectra were converted to mzXML using an extractor built upon
610 Thermo Fisher’s RAW File Reader library (version 4.0.26). In this extractor, the standard mzxml
611 format has been augmented with additional custom fields that are specific to ion trap and Orbitrap
612 mass spectrometry and essential for TMT quantitation. These additional fields include ion
613 injection times for each scan, Fourier Transform-derived baseline and noise values calculated for
614 every Orbitrap scan, isolation widths for each scan type, scan event numbers, and elapsed scan
615 times. This software is a component of the MassPike software platform and is licensed by Harvard
616 Medical School.

617 A combined database was constructed from (a) the human Uniprot database (4th February 2014),
618 (b) the BK polyomavirus database (6th October, 2014). The combined database was concatenated
619 with a reverse database composed of all protein sequences in reversed order. Searches were
620 performed using a 20 ppm precursor ion tolerance (41). Product ion tolerance was set to 0.03 Th.
621 TMT tags on lysine residues and peptide N termini (229.162932 Da) and carbamidomethylation of
622 cysteine residues (57.02146 Da) were set as static modifications, while oxidation of methionine
623 residues (15.99492 Da) was set as a variable modification.

624 To control the fraction of erroneous protein identifications, a target-decoy strategy was employed
625 (42, 43). Peptide spectral matches (PSMs) were filtered to an initial peptide-level false discovery
626 rate (FDR) of 1% with subsequent filtering to attain a final protein-level FDR of 1% (44, 45). PSM
627 filtering was performed using a linear discriminant analysis, as described previously (46). This
628 distinguishes correct from incorrect peptide IDs in a manner analogous to the widely used

629 Percolator algorithm (47), though employing a distinct machine learning algorithm. The following
630 parameters were considered: XCorr, ΔC_n , missed cleavages, peptide length, charge state, and
631 precursor mass accuracy. Protein assembly was guided by principles of parsimony to produce the
632 smallest set of proteins necessary to account for all observed peptides (46).

633 Proteins were quantified by summing TMT reporter ion counts across all matching peptide-
634 spectral matches using "MassPike", as described previously (39, 40). Briefly, a 0.003 Th window
635 around the theoretical m/z of each reporter ion (126, 127n, 127c, 128n, 128c, 129n, 129c, 130n,
636 130c, 131n, 131c) was scanned for ions, and the maximum intensity nearest to the theoretical m/z
637 was used. The primary determinant of quantitation quality is the number of TMT reporter ions
638 detected in each MS3 spectrum, which is directly proportional to the signal-to-noise (S:N) ratio
639 observed for each ion (48). Conservatively, every individual peptide used for quantitation was
640 required to contribute sufficient TMT reporter ions (minimum of ~1250 per spectrum) so that each
641 on its own could be expected to provide a representative picture of relative protein abundance (39).
642 An isolation specificity filter was additionally employed to minimise peptide co-isolation (49).
643 Peptide-spectral matches with poor quality MS3 spectra (more than 9 TMT channels missing
644 and/or a combined S:N ratio of less than 250 across all TMT reporter ions) or no MS3 spectra at
645 all were excluded from quantitation. Peptides meeting the stated criteria for reliable quantitation
646 were then summed by parent protein, in effect weighting the contributions of individual peptides
647 to the total protein signal based on their individual TMT reporter ion yields. Protein quantitation
648 values were exported for further analysis in Excel.

649 For protein quantitation, reverse and contaminant proteins were removed, then each reporter ion
650 channel was summed across all quantified proteins and normalised assuming equal protein loading
651 across all channels. For further analysis and display in figures, fractional TMT signals were used
652 (i.e. reporting the fraction of maximal signal observed for each protein in each TMT channel,
653 rather than the absolute normalized signal intensity). This effectively corrected for differences in
654 the numbers of peptides observed per protein. For all TMT experiments, normalised S:N values
655 are presented in Table S1 ('Data' worksheet).

656 Hierarchical centroid clustering based on uncentered Pearson correlation, and k-means clustering
657 were performed using Cluster 3.0 (Stanford University) and visualised using Java Treeview
658 (<http://jtreeview.sourceforge.net>) unless otherwise noted.

659

660 **Author Contributions**

661 L.G.C., R.A. and C.T.R.D. acquired and analysed the experimental data. L.G.C., C.T.R.D., P.J.L.,
662 M.P.W. and C.M.C. conceived and designed the experiments, interpreted the data and contributed
663 to writing the manuscript. M.P.W. and C.M.C. supervised the project.

664

665 **Competing Interests**

666 None of the authors have competing interests.

667

668 **Acknowledgments**

669 This work was supported by an Isaac Newton Trust / Wellcome Trust ISSF award to C.M.C., a
670 Biotechnology and Biological Sciences Research Council grant (BB/M021424/1) to C.M.C., a
671 Medical Research Council funded PhD studentship to L.G.C. and a Wellcome Trust Senior
672 Clinical Research Fellowship (108070/Z/15/Z) to M.P.W.

673

674 **References**

- 675 1. **Gardner SD, Field AM, Coleman DV, Hulme B.** 1971. NEW HUMAN PAPOVAVIRUS (BK) ISOLATED
676 FROM URINE AFTER RENAL TRANSPLANTATION. *Lancet* **1**:1253-&.
- 677 2. **Viscidi RP, Rollison DE, Sondak VK, Silver B, Messina JL, Giuliano AR, Fulp W, Ajidahun A,**
678 **Rivanera D.** 2011. Age-Specific Seroprevalence of Merkel Cell Polyomavirus, BK Virus, and JC
679 Virus. *Clinical and Vaccine Immunology* **18**:1737-1743.
- 680 3. **Huang G, Wu LW, Yang SC, Fei JG, Deng SX, Li J, Chen GD, Fu Q, Deng RH, Qiu J, Wang CX, Chen**
681 **LZ.** 2015. Factors Influencing Graft Outcomes Following Diagnosis of Polyomavirus - Associated
682 Nephropathy after Renal Transplantation. *PLoS One* **10**.
- 683 4. **Arthur RR, Shah KV, Baust SJ, Santos GW, Saral R.** 1986. ASSOCIATION OF BK VIRURIA WITH
684 HEMORRHAGIC CYSTITIS IN RECIPIENTS OF BONE-MARROW TRANSPLANTS. *New England Journal*
685 *of Medicine* **315**:230-234.
- 686 5. **Harris KF, Christensen JB, Imperiale MJ.** 1996. BK virus large T antigen: Interactions with the
687 retinoblastoma family of tumor suppressor proteins and on cellular growth control. *Journal of*
688 *Virology* **70**:2378-2386.
- 689 6. **Stubdal H, Zalvide J, Campbell KS, Schweitzer C, Roberts TM, DeCaprio JA.** 1997. Inactivation of
690 pRB-related proteins p130 and p107 mediated by the J domain of simian virus 40 large T antigen.
691 *Molecular and Cellular Biology* **17**:4979-4990.
- 692 7. **Lilyestrom W, Klein MG, Zhang RG, Joachimiak A, Chen XJS.** 2006. Crystal structure of SV40 large
693 T-antigen bound to p53: interplay between a viral oncoprotein and a cellular tumor suppressor.
694 *Genes & Development* **20**:2373-2382.
- 695 8. **Pallas DC, Shahrik LK, Martin BL, Jaspers S, Miller TB, Brautigan DL, Roberts TM.** 1990. POLYOMA
696 SMALL AND MIDDLE T-ANTIGENS AND SV40 SMALL T-ANTIGEN FORM STABLE COMPLEXES WITH
697 PROTEIN PHOSPHATASE-2A. *Cell* **60**:167-176.
- 698 9. **Scheidtmann KH, Mumby MC, Rundell K, Walter G.** 1991. DEPHOSPHORYLATION OF SIMIAN
699 VIRUS-40 LARGE-T ANTIGEN AND P53 PROTEIN BY PROTEIN PHOSPHATASE-2A - INHIBITION BY
700 SMALL-T ANTIGEN. *Molecular and Cellular Biology* **11**:1996-2003.
- 701 10. **Saribas AS, Coric P, Hamazaspian A, Davis W, Axman R, White MK, Abou-Gharbia M, Childers**
702 **W, Condra JH, Bouaziz S, Safak M.** 2016. Emerging From the Unknown: Structural and Functional
703 Features of Agnoprotein of Polyomaviruses. *Journal of Cellular Physiology* **231**:2115-2127.
- 704 11. **Panou M-M, Prescott EL, Hurdiss DL, Swinscoe G, Hollinshead M, Caller LG, Morgan EL, Carlisle L,**
705 **Mueller M, Antoni M, Kealy D, Ranson NA, Crump CM, Macdonald A.** 2018. Agnoprotein Is an

- 706 Essential Egress Factor during BK Polyomavirus Infection. *International Journal of Molecular*
707 *Sciences* **19**.
- 708 12. **Abend JR, Low JA, Imperiale MJ**. 2010. Global effects of BKV infection on gene expression in
709 human primary kidney epithelial cells. *Virology* **397**:73-79.
- 710 13. **Grinde B, Gayorfar M, Rinaldo CH**. 2007. Impact of a polyomavirus (BKV) infection on mRNA
711 expression in human endothelial cells. *Virus Research* **123**:86-94.
- 712 14. **Assetta B, De Cecco M, O'Hara B, Atwood WJ**. 2016. JC Polyomavirus Infection of Primary Human
713 Renal Epithelial Cells Is Controlled by a Type I IFN-Induced Response. *Mbio* **7**.
- 714 15. **An P, Robles MTS, Duray AM, Cantalupo PG, Pipas JM**. 2019. Human polyomavirus BKV infection
715 of endothelial cells results in interferon pathway induction and persistence. *Plos Pathogens* **15**.
- 716 16. **Justice JL, Verhalen B, Kumar R, Lefkowitz EJ, Imperiale MJ, Jiang MX**. 2015. Quantitative
717 Proteomic Analysis of Enriched Nuclear Fractions from BK Polyomavirus-Infected Primary Renal
718 Proximal Tubule Epithelial Cells. *Journal of Proteome Research* **14**:4413-4424.
- 719 17. **Weekes MP, Tomasec P, Huttlin EL, Fielding CA, Nusinow D, Stanton RJ, Wang Ecy, Aicheler R,
720 Murrell I, Wilkinson GWG, Lehner PJ, Gygi SP**. 2014. Quantitative Temporal Viomics: An
721 Approach to Investigate Host-Pathogen Interaction. *Cell* **157**:1460-1472.
- 722 18. **Huang DW, Sherman BT, Lempicki RA**. 2009. Systematic and integrative analysis of large gene lists
723 using DAVID bioinformatics resources. *Nature Protocols* **4**:44-57.
- 724 19. **Hornikova L, Fraiberk M, Man P, Janovec V, Forstova J**. 2017. VP1, the major capsid protein of
725 the mouse polyomavirus, binds microtubules, promotes their acetylation and blocks the host cell
726 cycle. *Febs Journal* **284**:301-323.
- 727 20. **Porras A, Gaillard S, Rundell K**. 1999. The simian virus 40 small-t and large-T antigens jointly
728 regulate cell cycle reentry in human fibroblasts. *Journal of Virology* **73**:3102-3107.
- 729 21. **Hesbacher S, Pfitzer L, Wiedorfer K, Angermeyer S, Borst A, Haferkamp S, Scholz CJ, Wobser M,
730 Schrama D, Houben R**. 2016. RB1 is the crucial target of the Merkel cell polyomavirus Large T
731 antigen in Merkel cell carcinoma cells. *Oncotarget* **7**:32956-32968.
- 732 22. **Orba Y, Suzuki T, Makino Y, Kubota K, Tanaka S, Kimura T, Sawa H**. 2010. Large T Antigen
733 Promotes JC Virus Replication in G(2)-arrested Cells by Inducing ATM- and ATR-mediated G(2)
734 Checkpoint Signaling. *Journal of Biological Chemistry* **285**:1544-1554.
- 735 23. **Papadimitriou JC, Randhawa P, Rinaldo CH, Drachenberg CB, Alexiev B, Hirsch HH**. 2016. BK
736 Polyomavirus Infection and Renourinary Tumorigenesis. *American Journal of Transplantation*
737 **16**:398-406.
- 738 24. **Sheppard HM, Corneillie SI, Espiritu C, Gatti A, Liu XA**. 1999. New insights into the mechanism of
739 inhibition of p53 by simian virus 40 large T antigen. *Molecular and Cellular Biology* **19**:2746-2753.
- 740 25. **Pines J, Hunter T**. 1991. HUMAN CYCLIN-A AND CYCLIN-B1 ARE DIFFERENTIALLY LOCATED IN THE
741 CELL AND UNDERGO CELL-CYCLE DEPENDENT NUCLEAR TRANSPORT. *Journal of Cell Biology* **115**:1-
742 17.
- 743 26. **Barak Y, Juven T, Haffner R, Oren M**. 1993. MDM2 EXPRESSION IS INDUCED BY WILD TYPE-P53
744 ACTIVITY. *Embo Journal* **12**:461-468.
- 745 27. **Wei CL, Wu Q, Vega VB, Chiu KP, Ng P, Zhang T, Shahab A, Yong HC, Fu YT, Weng ZP, Liu JJ, Zhao
746 XD, Chew JL, Lee YL, Kuznetsov VA, Sung WK, Miller LD, Lim B, Liu ET, Yu Q, Ng HH, Ruan YJ**.
747 2006. A global map of p53 transcription-factor binding sites in the human genome. *Cell* **124**:207-
748 219.
- 749 28. **Boehme KA, Blattner C**. 2009. Regulation of p53-insights into a complex process. *Critical Reviews*
750 *in Biochemistry and Molecular Biology* **44**:367-392.
- 751 29. **Vassilev LT, Vu BT, Graves B, Carvajal D, Podlaski F, Filipovic Z, Kong N, Kammlott U, Lukacs C,
752 Klein C, Fotouhi N, Liu EA**. 2004. In vivo activation of the p53 pathway by small-molecule
753 antagonists of MDM2. *Science* **303**:844-848.
- 754 30. **Jiang MX, Zhao LB, Gamez M, Imperiale MJ**. 2012. Roles of ATM and ATR-Mediated DNA Damage
755 Responses during Lytic BK Polyomavirus Infection. *Plos Pathogens* **8**.
- 756 31. **Verhalen B, Justice JL, Imperiale MJ, Jiang MX**. 2015. Viral DNA Replication-Dependent DNA
757 Damage Response Activation during BK Polyomavirus Infection. *Journal of Virology* **89**:5032-5039.

- 758 32. **Rundell K, Parakati R.** 2001. The role of the SV40ST antigen in cell growth promotion and
759 transformation. *Seminars in Cancer Biology* **11**:5-13.
- 760 33. **Chellappan SP, Hiebert S, Mudryj M, Horowitz JM, Nevins JR.** 1991. THE E2F TRANSCRIPTION
761 FACTOR IS A CELLULAR TARGET FOR THE RB PROTEIN. *Cell* **65**:1053-1061.
- 762 34. **Orba Y, Sunden Y, Suzuki T, Nagashima K, Kimura T, Tanaka S, Sawa H.** 2008. Pharmacological
763 cdk inhibitor R-Roscovitine suppresses JC virus proliferation. *Virology* **370**:173-183.
- 764 35. **Obaya AJ, Sedivy JM.** 2002. Regulation of cyclin-Cdk activity in mammalian cells. *Cellular and*
765 *Molecular Life Sciences* **59**:126-142.
- 766 36. **Holcakova J, Muller P, Tomasec P, Hrstka R, Nekulova M, Krystof V, Strnad M, Wilkinson GWG,**
767 **Vojtesek B.** 2014. Inhibition of Post-Transcriptional RNA Processing by CDK Inhibitors and Its
768 Implication in Anti-Viral Therapy. *PLoS One* **9**.
- 769 37. **Jiang MX, Abend JR, Tsai B, Imperiale MJ.** 2009. Early Events during BK Virus Entry and
770 Disassembly. *Journal of Virology* **83**:1350-1358.
- 771 38. **Evans GL, Caller LG, Foster V, Crump CM.** 2015. Anion homeostasis is important for non-lytic
772 release of BK polyomavirus from infected cells. *Open Biology* **5**.
- 773 39. **McAlister GC, Huttlin EL, Haas W, Ting L, Jedrychowski MP, Rogers JC, Kuhn K, Pike I, Grothe RA,**
774 **Blethrow JD, Gygi SP.** 2012. Increasing the Multiplexing Capacity of TMTs Using Reporter Ion
775 Isotopologues with Isobaric Masses. *Analytical Chemistry* **84**:7469-7478.
- 776 40. **McAlister GC, Nusinow DP, Jedrychowski MP, Wuehr M, Huttlin EL, Erickson BK, Rad R, Haas W,**
777 **Gygi SP.** 2014. MultiNotch MS3 Enables Accurate, Sensitive, and Multiplexed Detection of
778 Differential Expression across Cancer Cell Line Proteomes. *Analytical Chemistry* **86**:7150-7158.
- 779 41. **Haas W, Faherty BK, Gerber SA, Elias JE, Beausoleil SA, Bakalarski CE, Li X, Villen J, Gygi SP.** 2006.
780 Optimization and use of peptide mass measurement accuracy in shotgun proteomics. *Molecular &*
781 *Cellular Proteomics* **5**:1326-1337.
- 782 42. **Elias JE, Gygi SP.** 2007. Target-decoy search strategy for increased confidence in large-scale
783 protein identifications by mass spectrometry. *Nature Methods* **4**:207-214.
- 784 43. **Elias JE, Gygi SR.** 2010. Target-Decoy Search Strategy for Mass Spectrometry-Based Proteomics.
785 *Proteome Bioinformatics* **604**:55-71.
- 786 44. **Kim W, Bennett EJ, Huttlin EL, Guo A, Li J, Possemato A, Sowa ME, Rad R, Rush J, Comb MJ,**
787 **Harper JW, Gygi SP.** 2011. Systematic and Quantitative Assessment of the Ubiquitin-Modified
788 Proteome. *Molecular Cell* **44**:325-340.
- 789 45. **Wu R, Dephoure N, Haas W, Huttlin EL, Zhai B, Sowa ME, Gygi SP.** 2011. Correct Interpretation of
790 Comprehensive Phosphorylation Dynamics Requires Normalization by Protein Expression
791 Changes. *Molecular & Cellular Proteomics* **10**.
- 792 46. **Huttlin EL, Jedrychowski MP, Elias JE, Goswami T, Rad R, Beausoleil SA, Villen J, Haas W, Sowa**
793 **ME, Gygi SP.** 2010. A Tissue-Specific Atlas of Mouse Protein Phosphorylation and Expression. *Cell*
794 **143**:1174-1189.
- 795 47. **Kall L, Canterbury JD, Weston J, Noble WS, MacCoss MJ.** 2007. Semi-supervised learning for
796 peptide identification from shotgun proteomics datasets. *Nature Methods* **4**:923-925.
- 797 48. **Makarov A, Denisov E.** 2009. Dynamics of Ions of Intact Proteins in the Orbitrap Mass Analyzer.
798 *Journal of the American Society for Mass Spectrometry* **20**:1486-1495.
- 799 49. **Ting L, Rad R, Gygi SP, Haas W.** 2011. MS3 eliminates ratio distortion in isobaric multiplexed
800 quantitative proteomics. *Nature Methods* **8**:937-940.
- 801 50. **Cox J, Mann M.** 2008. MaxQuant enables high peptide identification rates, individualized p.p.b.-
802 range mass accuracies and proteome-wide protein quantification. *Nature Biotechnology* **26**:1367-
803 1372.

804

805 Figure Legends

806 **Figure 1. Quantitative temporal analysis of BK virus lytic infection.**

- 807 (A) Schematic of experimental workflow. RPTE and HU cells were infected at MOI 5 or mock
808 infected. Whole cell lysates (WCL) were harvested at 24, 48, and 72 h (infected samples)
809 or 24 and 72 h (mock infected samples).
810 (B) Hierarchical cluster analysis of all quantified proteins.
811 (C) Scatter plots of all proteins quantified at 24, 48 and 72 hpi in RPTE and HU cells. Fold
812 change is shown in comparison to the average corresponding mock for the same cell type.
813 Benjamini-Hochberg-corrected significance B was used to estimate p-values (50).
814 (D) Scatter plot showing the correlation between protein abundance changes in BKPyV
815 infected RPTE and HU cells, and overlap of proteins up and downregulated by > 2-fold
816 between RPTE and HU cells.
817 (E) Temporal profiles of the 5 viral proteins identified, normalised to a maximum of one.
818

819 **Figure 2. Repeat quantitative temporal profiling in RPTE cells (Experiment 2).**

- 820 (A) Schematic of experimental workflow for experiment 2.
821 (B) Scatter plots of all proteins quantified. Fold change is shown in comparison to the average
822 corresponding mock. Benjamini-Hochberg-corrected significance B was used to estimate
823 p-values (Cox and Mann, 2008).
824 (C) Overlap of proteins quantified between Experiment 1 and Experiment 2.
825 (D) Scatter plot showing the correlation between experiments 1 and 2 in RPTE cells, for
826 proteins quantified by ≥ 2 -peptides.
827 (E) Temporal profiles of the 5 viral proteins quantified, normalised to a max of one.
828

829 **Figure 3. Proteins involved in the innate antiviral immune response remain unchanged**
830 **during BKPyV infection.**

- 831 (A) Up- or down-regulation of a minority of proteins with innate antiviral function (Uniprot
832 keywords: 'Innate immunity' and 'Antiviral').
833 (B) Example protein profiles from (A).
834 (C) Validation of temporal profiles shown in (B) by Western blot. RPTE cells were mock
835 infected or infected with BKPyV at MOI 3 or stimulated with IFN α 2A (10^4 U/mL) and
836 analysed by Western blot for the proteins shown.
837

838 **Figure 4. RPTE cells phosphorylate and translocate IRF3 in response to cytoplasmic RNA**
839 **and DNA but fail to do so upon BKPyV infection.**

- 840 (A) Immunofluorescence microscopy analysis of IRF3 localisation changes upon stimulation.
841 RPTE cells infected with BKPyV (MOI 0.5) or mock infected were fixed at 48 hpi. RPTE
842 cells stimulated with Poly I:C (2 μ g/mL) or stimulatory DNA (2 μ g/mL) were fixed at 6 h
843 after stimulation. DAPI was used as a nuclear marker and anti-VP1 as a marker of
844 infection.
845 (B) Analysis of IRF3 phosphorylation by Western blot. RPTE cells infected with BKPyV
846 (MOI 3) or mock infected and harvested at 48 hpi. RPTE cells stimulated with Poly I:C (2
847 μ g/mL) or stimulatory DNA (2 μ g/mL) were harvested at 6 h after stimulation.
848

849 **Figure 5. BKPyV and mock-infected RPTE cells do not differ in their responses to**
850 **cytoplasmic RNA and DNA.**

- 851 (A) Immunofluorescence microscopy analysis of IRF3 localisation changes upon stimulation in
852 BKPyV infected or uninfected cells. RPTE cells infected with BKPyV (MOI 0.5) or mock
853 infected were stimulated with Poly I:C (2 μ g/mL) or oligomeric DNA (2 μ g/mL) at 42 hpi
854 and fixed at 48 hpi. DAPI was used as a nuclear marker and anti-LTAg as a marker of
855 infection.
856 (B) Analysis of IRF3 phosphorylation upon stimulation in BKPyV infected or uninfected cells
857 by Western blot. RPTE cells infected with BKPyV (MOI 3) or mock infected were

858 stimulated with Poly I:C (2 µg/mL) or oligomeric DNA (2 µg/mL) at 42 hpi and fixed at 48
859 hpi.

860

861 **Figure 6. Upregulated proteins are enriched in cell cycle functions.**

862 (A) DAVID enrichment analysis of proteins upregulated or downregulated >2-fold against a
863 background of all 8985 human proteins quantified in Experiment 1. No significantly
864 enriched downregulated clusters were observed for HU cells.

865 (B) Example protein profiles for selected cell cycle-related proteins for both RPTE and HU
866 cells. Proteins families are separated by coloured boxes.

867 (C) Validation of selected temporal profiles shown in (B) by Western blot (RPTE cells, MOI
868 3). Tubulin was used as a loading control and VP1 as a control for infection.

869

870 **Figure 7. MDM2 and p53 are modulated by BKPyV via LTA_g-dependent and -independent
871 activities.**

872 (A) Expression of MDM2, p53 and LTA_g in RPTE cells infected with BKPyV (MOI 1) or
873 mock infected, then treated with 5 µM Nutlin-3 or DMSO as a control at 2 hpi, fixed at 48
874 hpi. DAPI was used as a nuclear marker.

875 (B) Expression of MDM2, p53 and LTA_g in RPTE cells transfected with BKPyV LTA_g, then
876 treated with 5 µM Nutlin-3 or DMSO as a control at 2 h and subjected to cell cycle
877 inhibition (RO-3306 5 µM) at 24 h, fixed at 48 h post transfection. DAPI was used as a
878 nuclear marker. Five example cells shown for each condition

879

880 **Figure 8. Cell cycle inhibitors have variable effects on BKPyV induced G2/M phase cell cycle
881 arrest.**

882 (A) The cell cycle status of RPTE cells was determined in a number of different experimental
883 conditions. RPTE cells were infected with BKPyV (MOI 3) or mock infected, then
884 subjected to CDK4/6 inhibition (PD0332991 1 µM), CDK1/2 inhibition (Roscovitine 20
885 µM) or CDK1 inhibition (RO-3306 5 µM) at 24 hpi, and subsequently collected for
886 analysis at 48 hpi. Collected cells were stained with propidium iodide (PI) and analysed by
887 flow cytometry (n=3). Error bars represent standard deviation. *p < 0.05; **p < 0.01; ***p
888 < 0.001; ns = not significant; two sample t-test for changes in proportion of cells in G1.

889 (B) Histograms of PI stain for each experimental condition of a single experiment shown.

890 (C) Cell viability tests. RPTE cells were treated with 1 µM PD0332991, 20 µM Roscovitine or
891 5 µM RO-3306 for 24 h then subjected to a Trypan Blue exclusion assay according to
892 manufacturers protocol (n=3).

893

894 **Figure 9. CDK1 and 2 inhibitors impede BKPyV replication in RPTE cells.**

895 RPTE cells infected with BKPyV (MOI=3) were subjected to CDK4/6 inhibition (1 µM
896 PD0332991), CDK1/2 inhibition (20 µM Roscovitine) or CDK1 inhibition (5 µM RO-
897 3306) from 24 hpi and harvested for analysis at 48 hpi.

898 (A) qPCR to determine viral DNA copy numbers per cell. DNA was extracted from each
899 condition, BKPyV genome copy number was determined, normalised to host gene (TNFα)
900 copy number and compared to the uninhibited control, which was arbitrarily set to 1 (n=6).

901 (B) Expression of viral proteins VP1, VP2, VP3, Agno, and LTA_g was determined by Western
902 blot. Tubulin was used as a loading control.

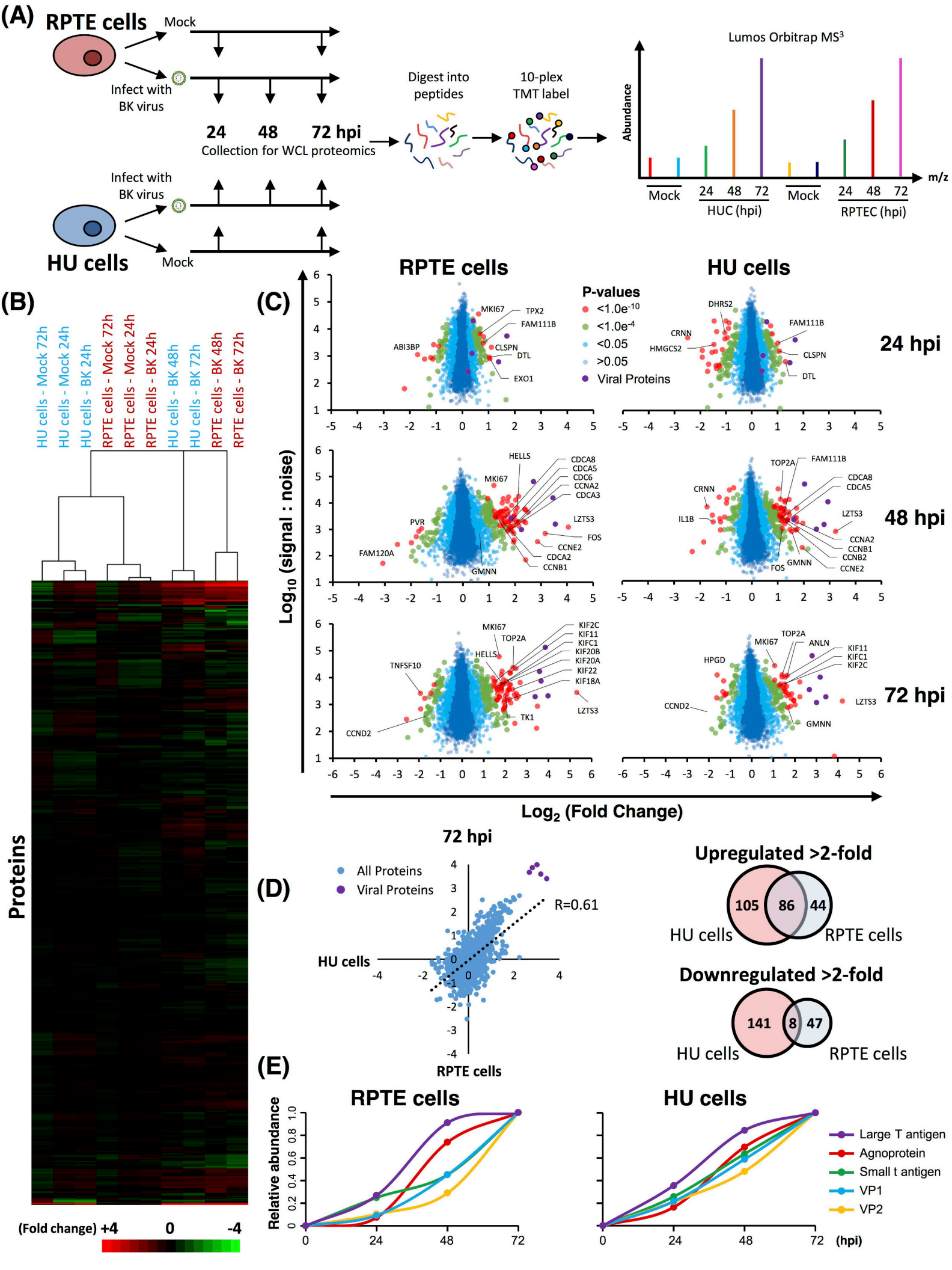
903 (C) Infectious BKPyV produced in each experimental condition was determined by fluorescent
904 focus unit (FFU) assay and normalised to uninhibited control (arbitrarily set to 1) (n=7).

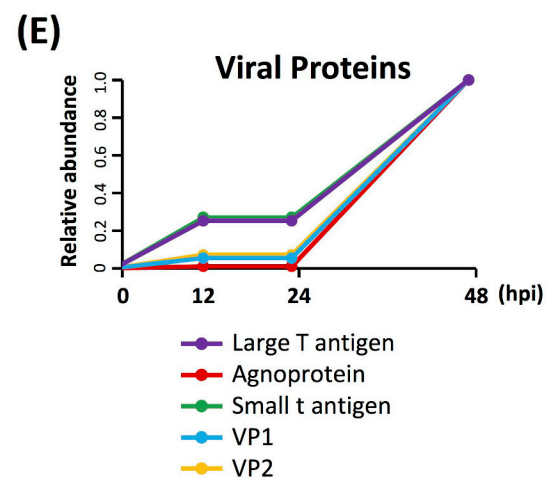
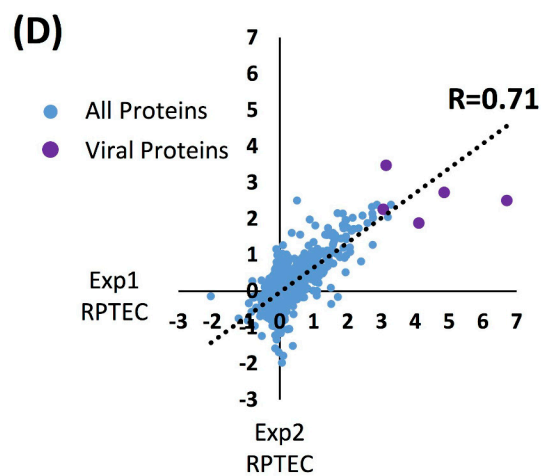
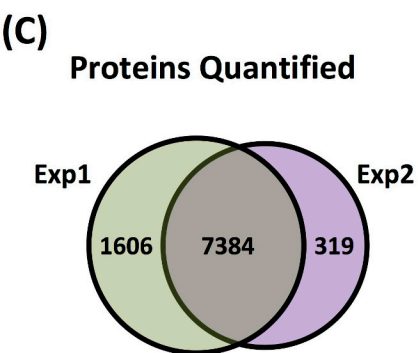
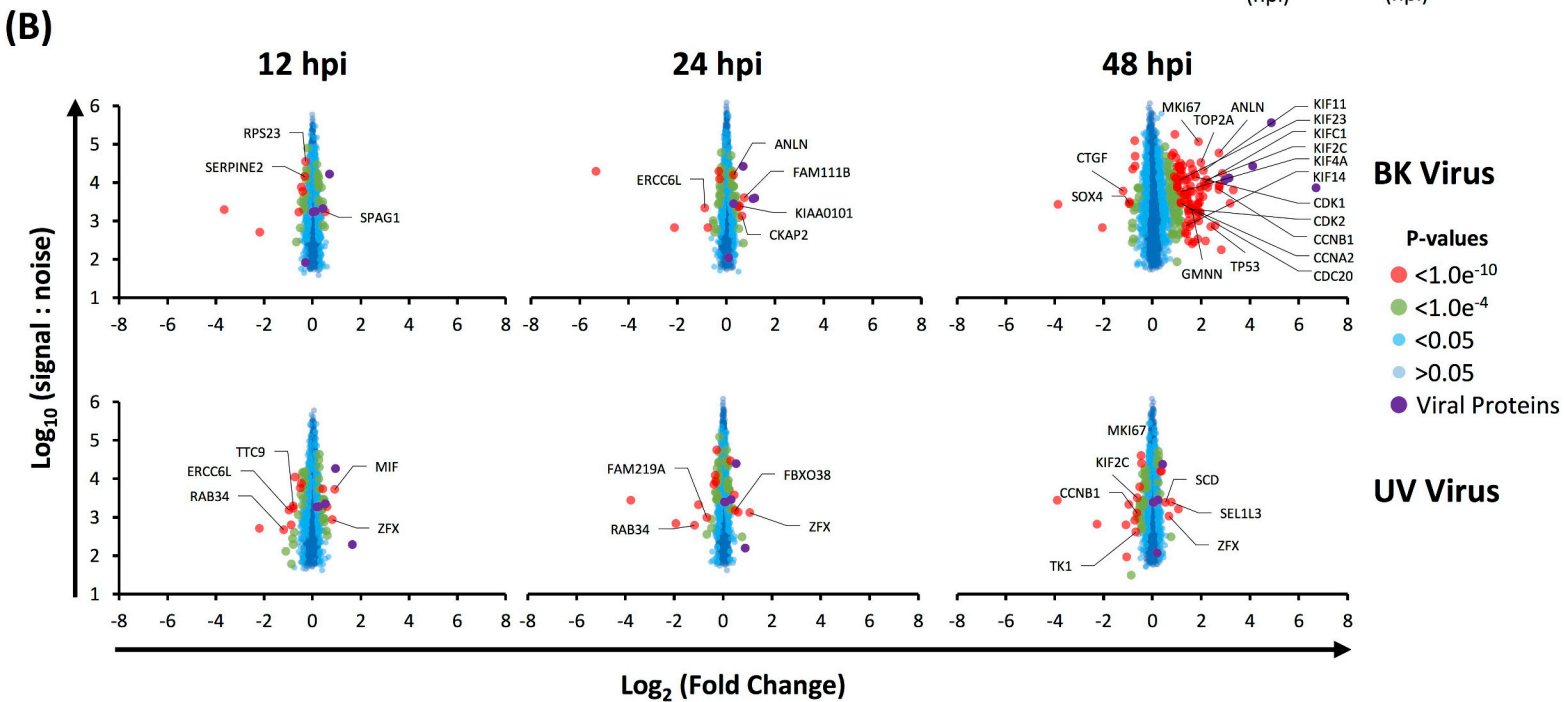
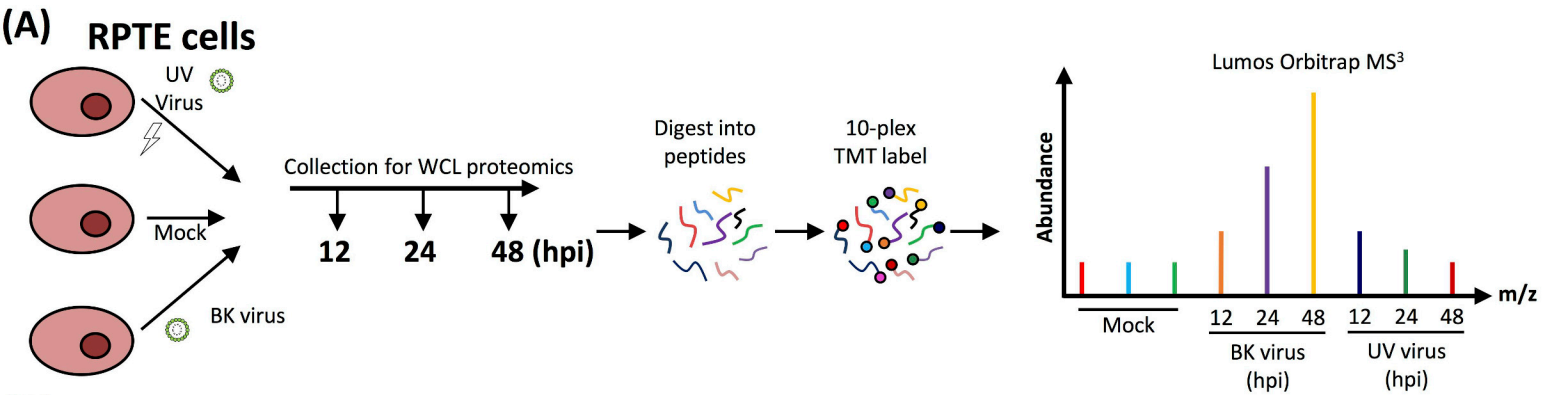
905 Error bars represent standard deviation. *p < 0.05; ***p < 0.001; ****p < 0.0001; ns = not
906 significant; one sample t-test experimental conditions versus control.

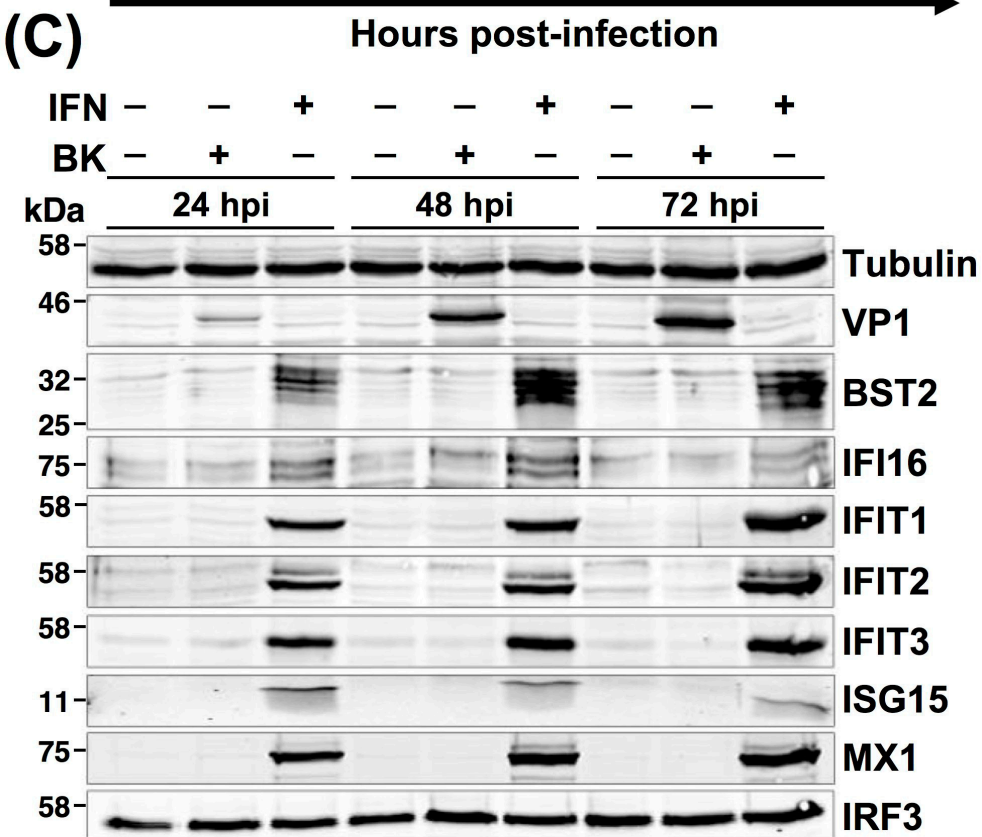
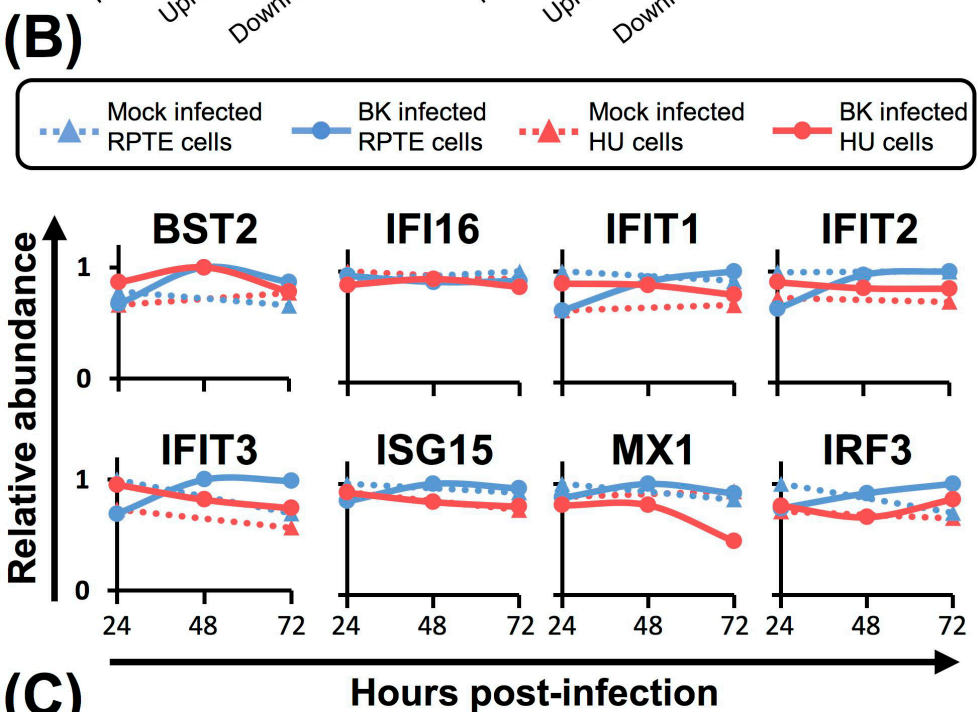
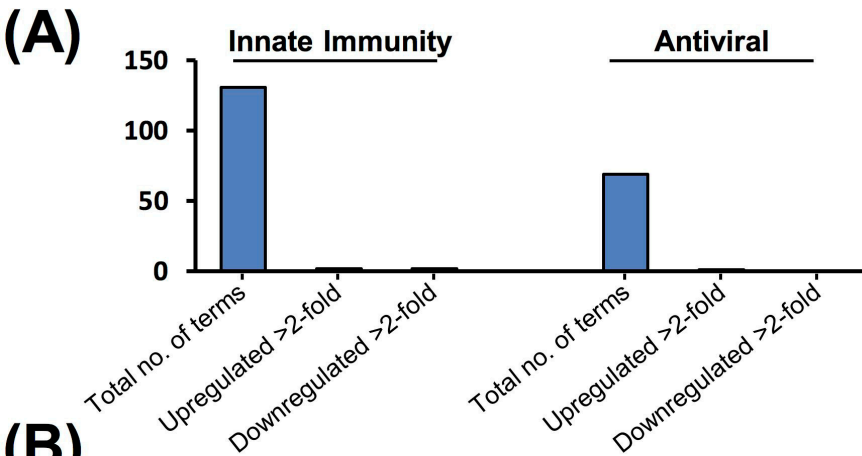
907

908 **Figure 10. Proposed mechanism of interplay between MDM2 and p53 levels in the presence
909 of LTA_g**

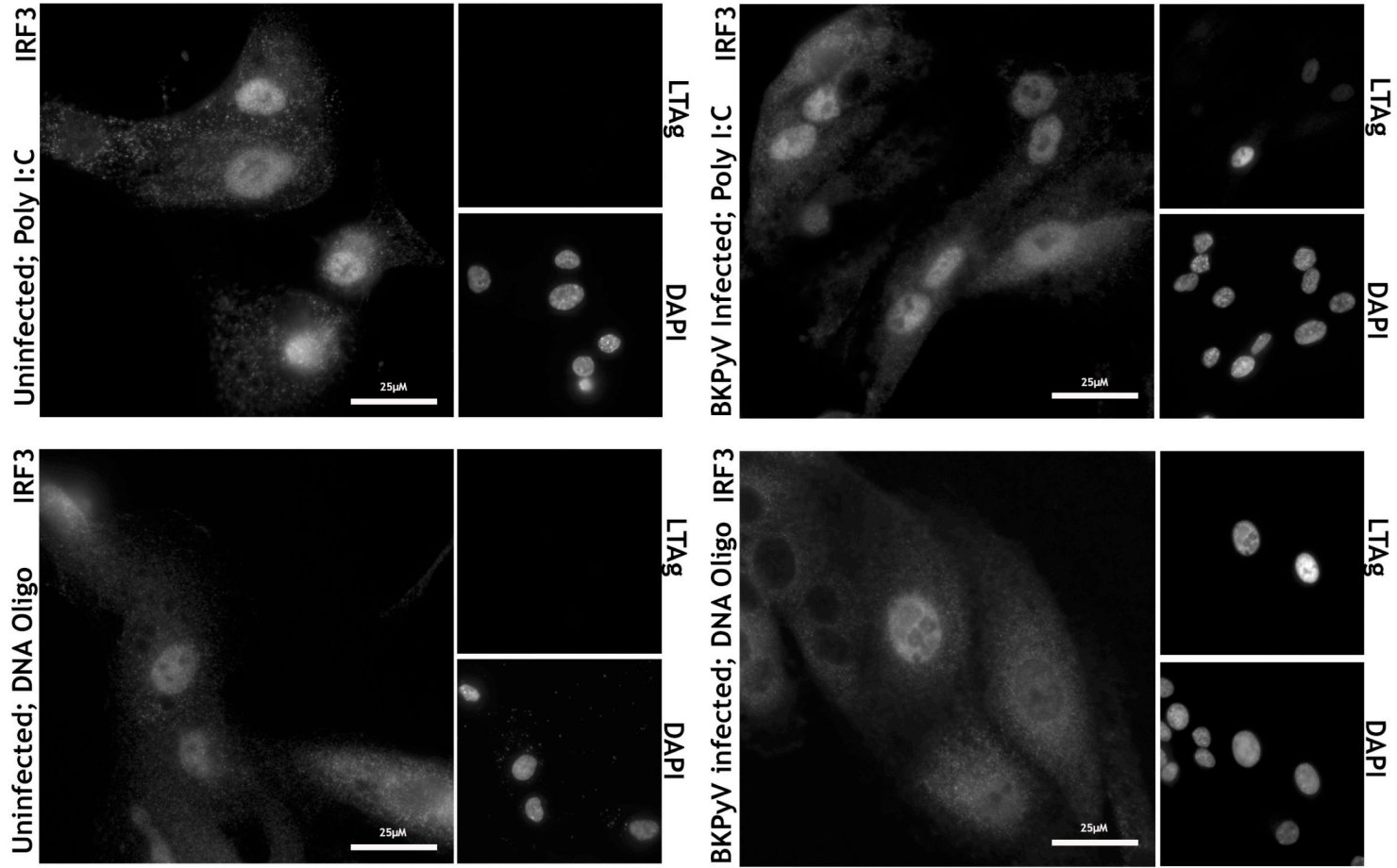
- 910 (A) Untreated cells.
911 (B) Uninfected, untransfected cells inhibited with Nutlin-3.
912 (C) Cells expressing LTA_g in the absence of infection.
913 (D) Cells BKPyV infected, or cells expressing LTA_g combined with cell cycle arrest/DNA
914 damage.
915



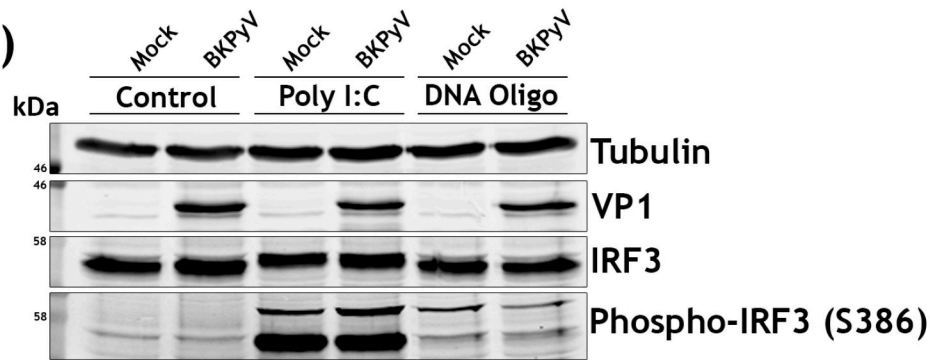


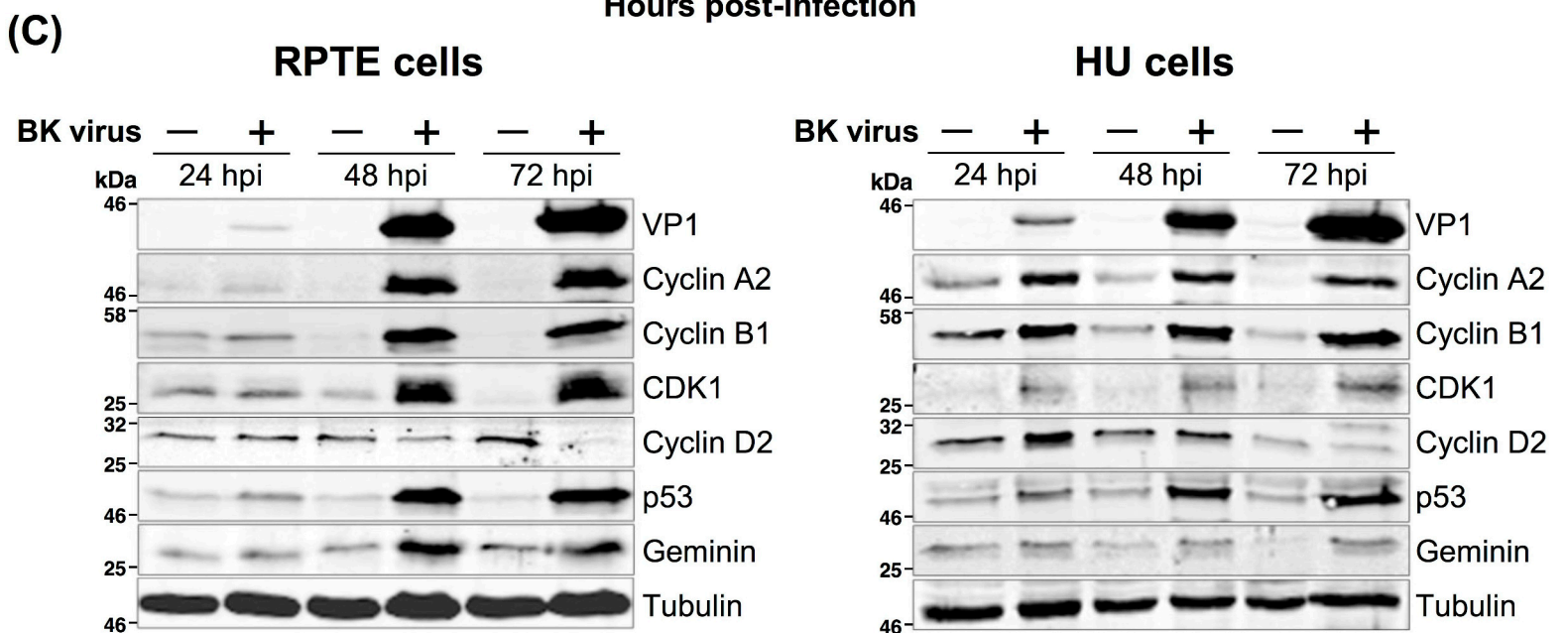
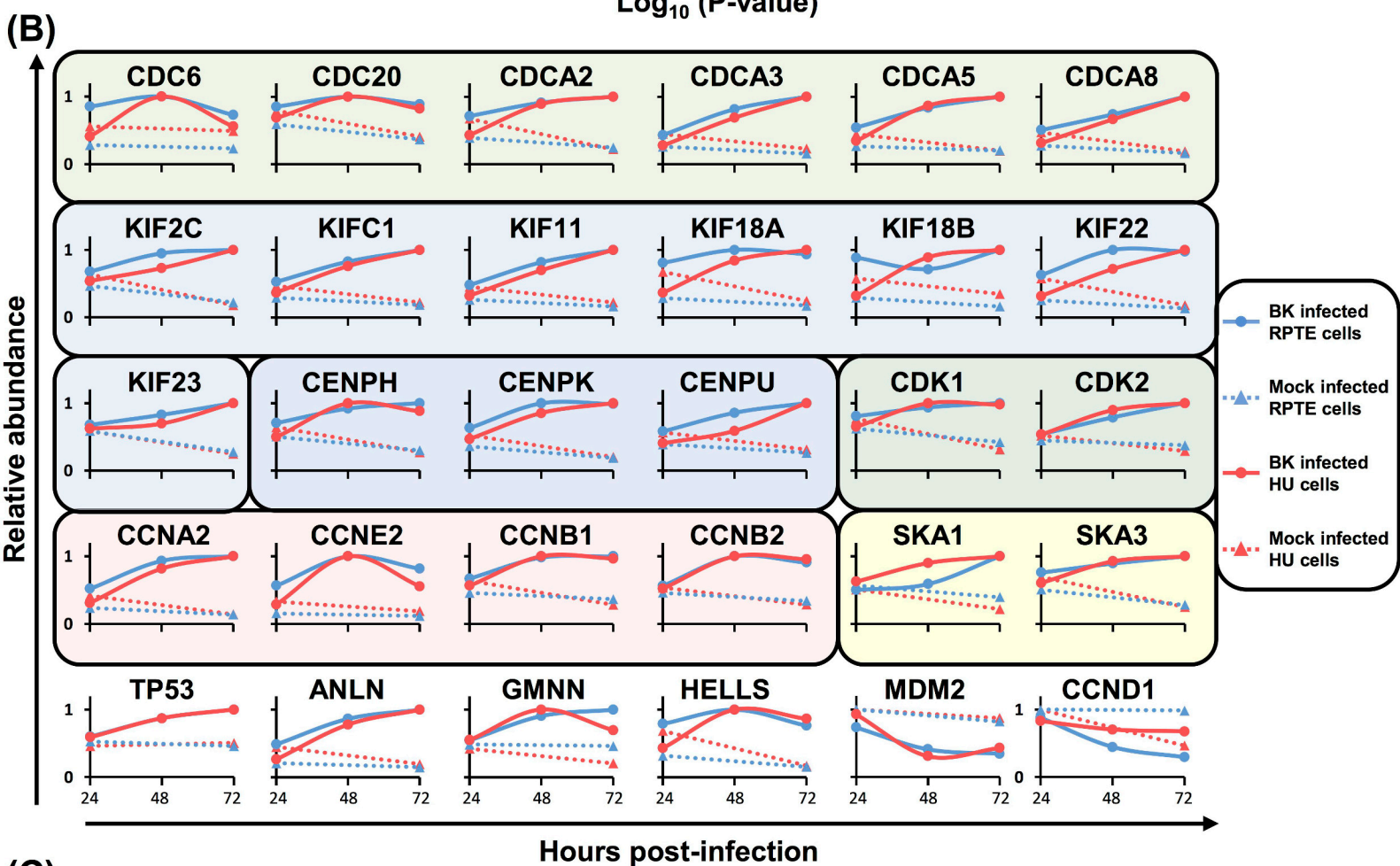
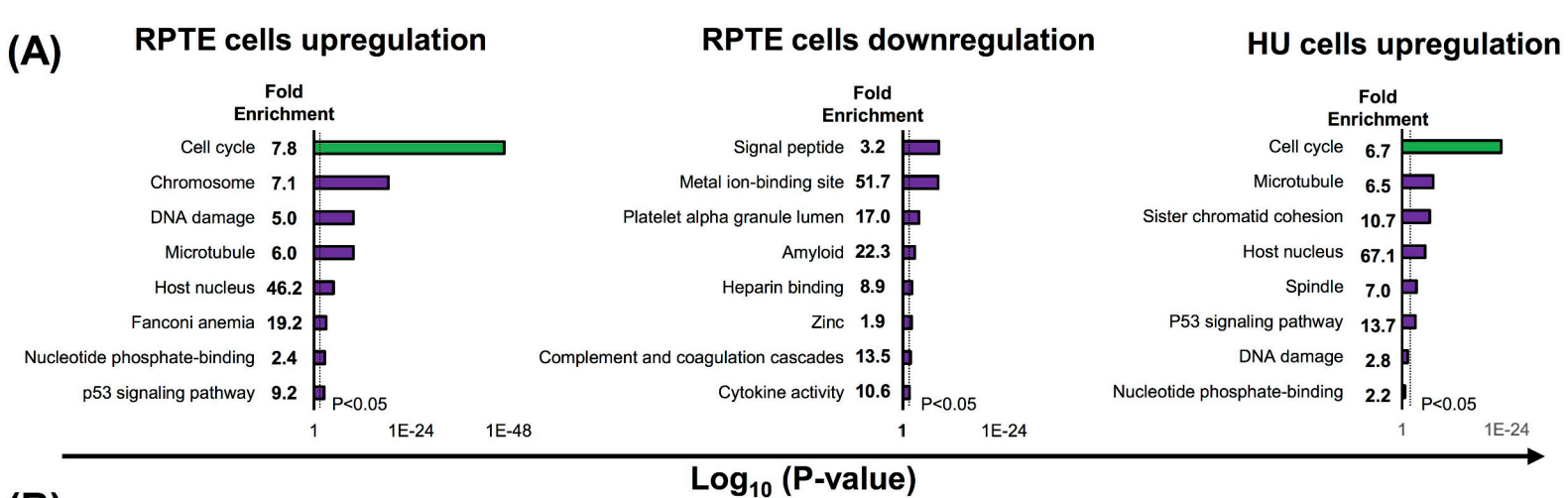


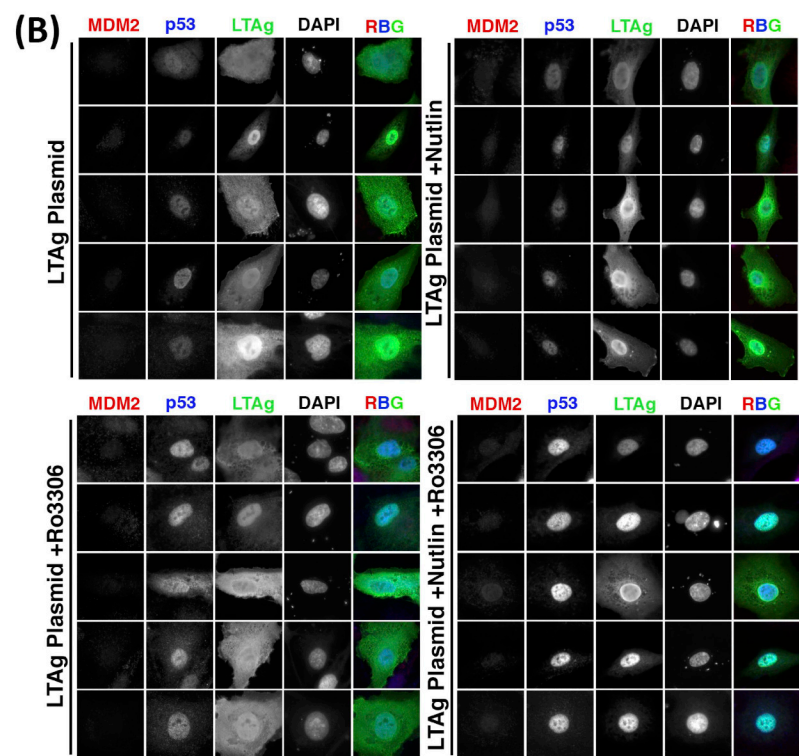
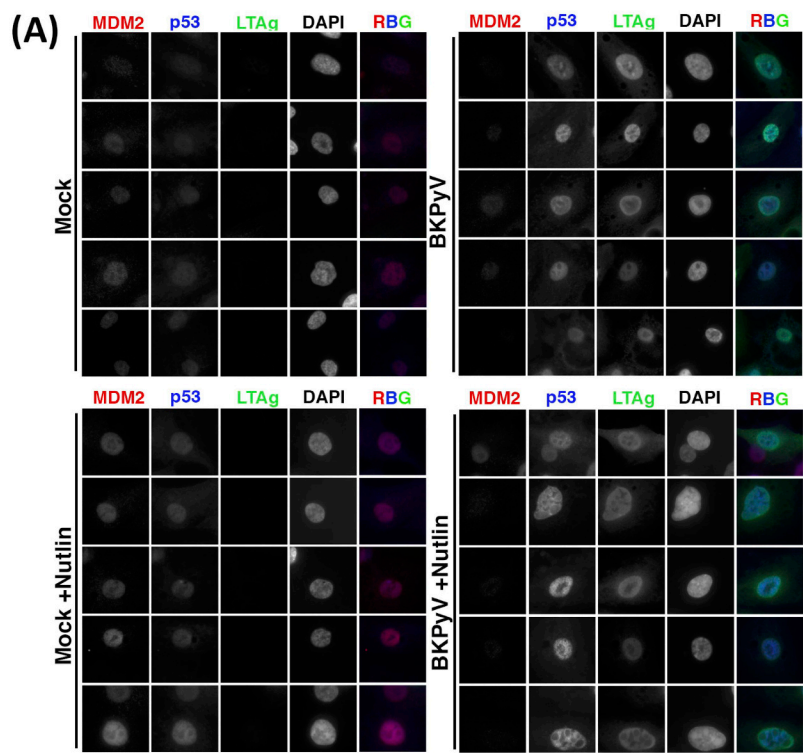
(A)

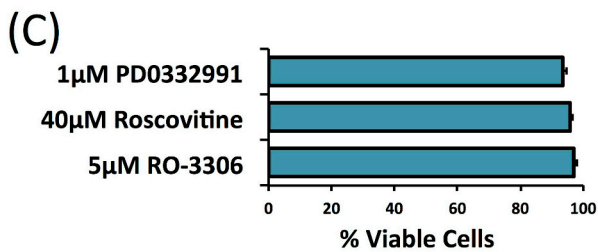
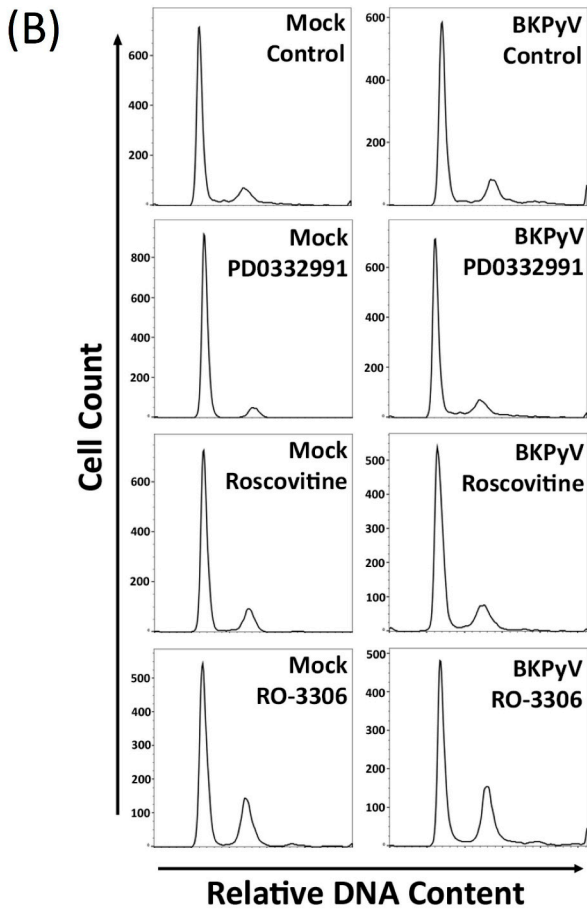
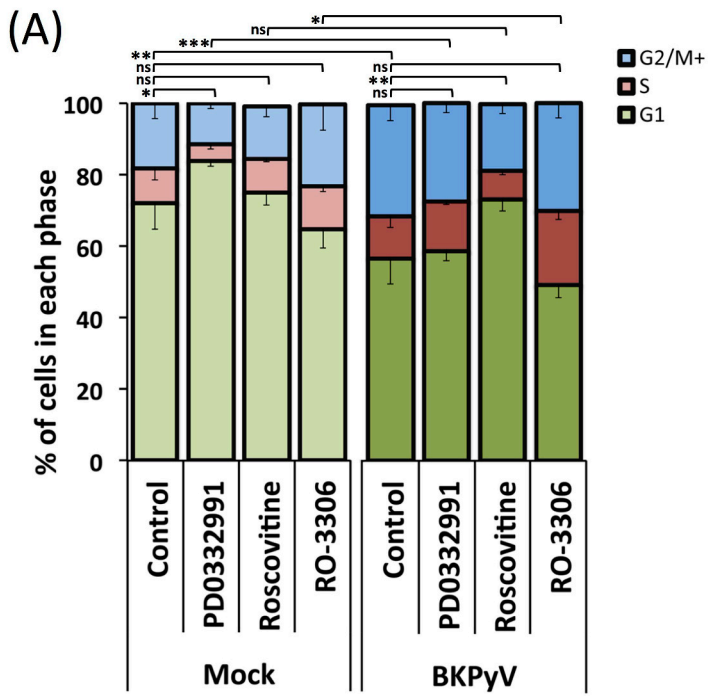


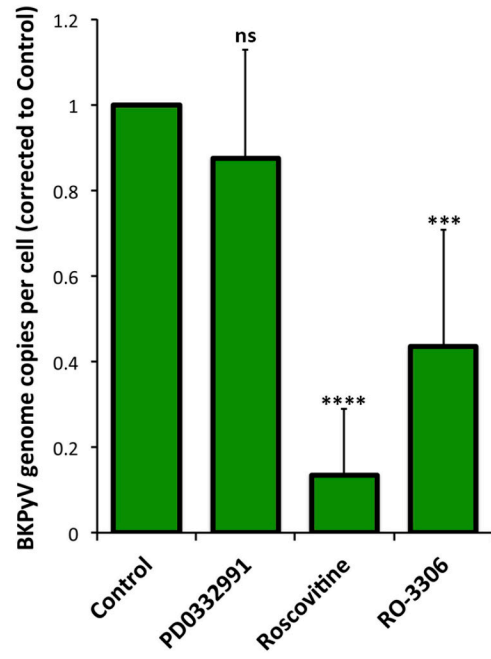
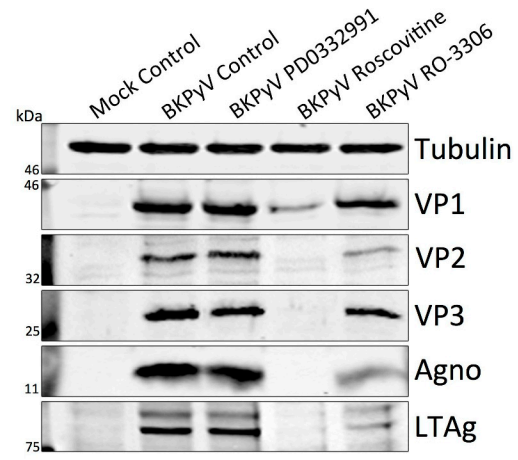
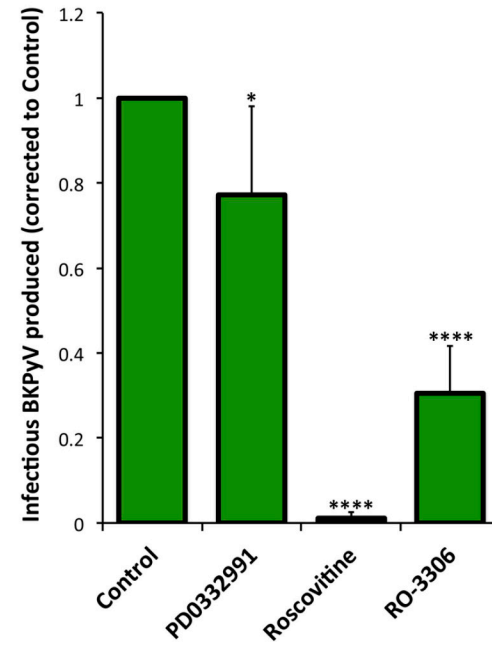
(B)



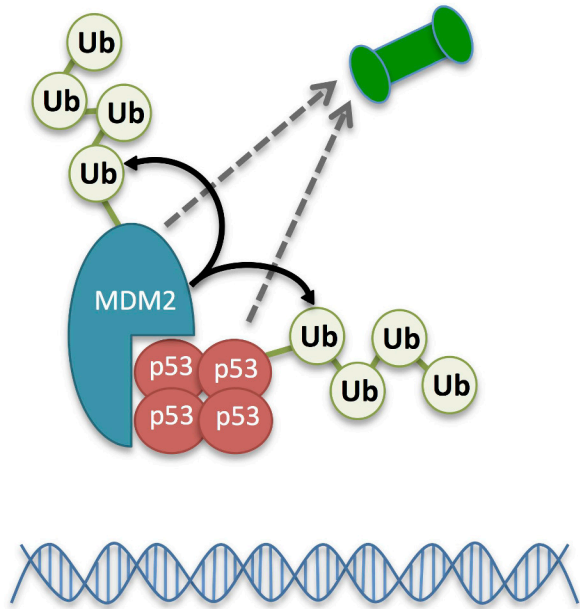




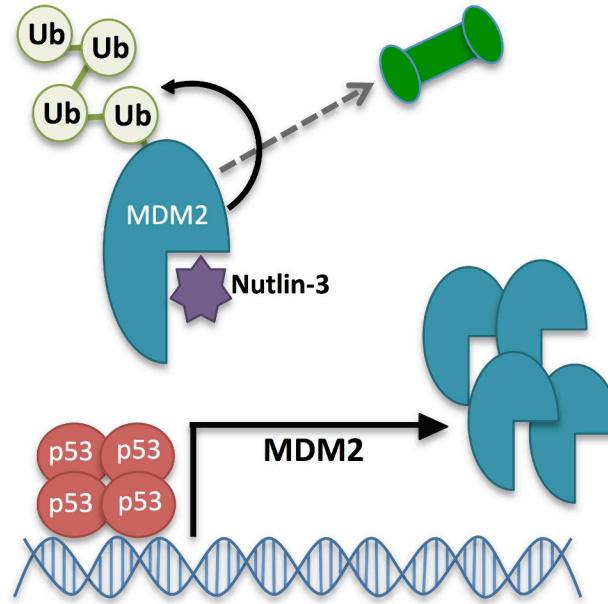


(A)**(B)****(C)**


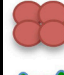





(A)



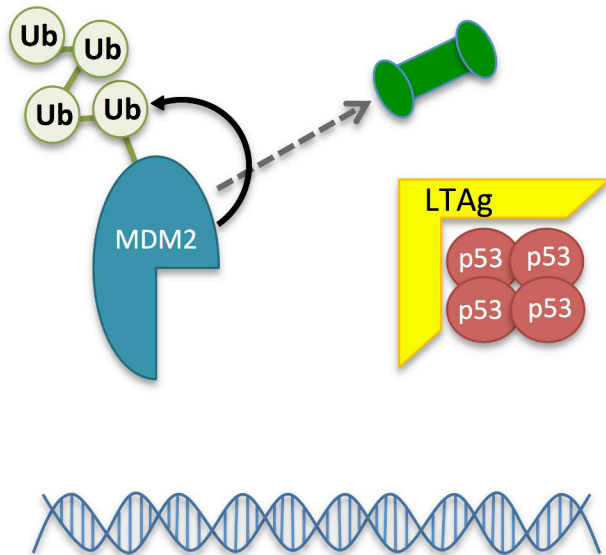
(B)



KEY:

-  MDM2
-  p53
-  Proteasome
-  Nutlin-3
-  LTAg
-  BKPyV Infection
-  DNA Damage/
Cell Cycle Arrest

(C)



(D)

